The State Scientific Center
of Russia Federation
Budker Institute of Nuclear Physics
Siberian Branch of Russian Academy of Science

A.I.Gorbovsky, V.V.Mishagin, V.H.Lev, V.Y.Kremyansky, A.V.Sitnikov,
K.K.Schreiner, M.V.Tauber, G.F.Abdrashitov, A.V.Anikeev, E.D.Bender,
P.A.Bagryansky, A.A.Ivanov, A.N.Karpushov, A.M.Kudryavtsev,
I.A.Kotel'nikov, E.P.Kruglyakov, I.M.Lansky, A.A.Pod'minogin,
V.M.Panasyuk, S.D.Kravchenko, V.N.Bocharov, S.G.Konstantinov,
O.K.Myskin, A.I.Rogozin, D.D.Ryutov, Yu.S.Popov, V.I.Volosov,
Yu.N.Yudin, and Yu.A.Tsidulko
Budker Institute of Nuclear Physics, 630090, Novosibirsk, Russia

H.Kumpf, K.Noack, G.Otto, St.Krahl
Forschungszentrum Rossendorf e.V., Germany

V.Robouch
ENEA Frascati, Italy

HYDROGEN PROTOTYPE OF A PLASMA NEUTRON SOURCE

BudkerINP 95-90

Novosibirsk
1995

Contents

© Budker Institute of Nuclear Physics, Russia

Introduction

The present research has been done to develop main design solutions for the Hydrogen Prototype of the Neutron Source (acronym HPNS) based on a gas-dynamic trap concept. As a main part, it includes a design of the magneto-vacuum system of the device. Also presented here are the neutral beam duct designs. The paper is organized as follows: Section 1 is devoted to the general description of the gas-dynamic trap concept and its application to an intense neutron source design. Main goals of the HPNS experimental program as well as the target parameters of the facility are given in Section 2. General layout of HPNS and operational scenarios are presented in Section 3. Sections 4.1-4.4 describe the technical design features of the main subsystems of HPNS: magnets, vacuum system, NB-injectors and the target plasma build-up system. The subsection devoted to the magnets gives a description of the central cell coil set and presents calculated parameters of the magnetic field. Here the characteristics of the chosen power supply for the magnets are described too. A technology for manufacturing the coils in the INP machine shop is also briefly discussed in this subsection. Here is also given the design of mirror magnets. These magnets produce on-axis magnetic field of about 20 Tesla and operate under extremely strong ponderomotive forces. Therefore their design has to be different from that of the central cell coils.

We considered a layout where the magnets are composed of outer and inner sections. The first one is powered in series with the central cell coils while the inner small radius insert is independently energized from a capacitor bank in 150 ms pulses. The heat released during the pulse is removed between shots by air cooling from the side walls of the inserts. Such a realization allows the mirror ratio to be variable in the range from 8 to 20. The vacuum system of the Hydrogen Prototype is discussed in a separate subsection. It is worthwhile to note that after the design had been started, almost from the very beginning we recognized that magnets and vacuum system cannot be designed separately. For example, which is probably the most simple one, periodical baking of the main vacuum chamber demands for the coils to be thermally and mechanically insulated from the chamber. The subsection devoted to the vacuum system also describes the structure of the first wall and plasma dump design. Also described here are the remotely controlled plasma limiters which are located inside the central cell vacuum chamber. The final section presents the supplementing simulation models and alternative MHD-anchor studies.

1. GDT concept and its application to a neutron source design.

A gas-dynamic trap concept has been proposed recently /1,2/ as a possible approach to an open-ended reactor or a 14MeV neutron source for use in accelerated material tests /3,4/. The gas-dynamic trap (GDT) is an axisymmetric mirror confinement device with a mirror ratio $R_m >> 1$ and a lenght L which exceeds the ion mean free-path of scattering into loss cone (angle of scattering $1/\sqrt{R_m}$). In the gas-dynamic trap, the central cell ions are lost out of the ends at the rate determined by an ion acoustic speed - V_{Ti}. The resulting collisional plasma lifetime can then be roughly estimated as $R_m L / V_{Ti}$. For stability reasons it is important that under these conditions plasma extends significantly into the regions outside the magnetic mirrors. Beyond the mirrors the expanding field lines are concave outwards which is favorable for plasma stability. By adjusting the magnetic field at the mirror throats, the plasma density inside these regions can be increased above a certain value, so as to make the pressure-weighted curvature averaged over the entire trap favorable for MHD-stability. This stability has been successfully demonstrated in recent experiments on the GDT facility at moderate plasma parameters /5/.

One of the most attractive application of such a system to controlled fusion is a neutron source for testing candidate core materials for a fusion reactor /6/. This source utilises the "beam-plasma target" approach which was first succesfully applied in 2XIIB experiment in LLNL /7/. This approach appeared to be particularly fruitful in the case of a mirror-based neutron source /3,8/. To be used as a neutron source, a multi-component version of GDT is the most convenient. A two component GDT is operated with a relatively cold dense deuterium plasma ($T \approx$ 0.5-1.0keV) and a fast tritium ion minority ($\approx$ 200keV energy) produced by oblique injection of energetic neutral beams at the center of the device. A schematic view of a GDT-based neutron source is shown on Fig.1

Interacting with a relatively cold target plasma, the fast ion distribution is formed mainly by ions slowing down by electron drag /3/. The fast ion drag prevent appreciable pitch angle broadening of the initially injected beam. Under such a condition their angular spread is kept close to that of primary neutrals which can be made rather narrow. Thus the fast ions are confined in the mirror region inside of which their longitudinal density profile is strongly nonhomogenious. Due to small angular spread in the vicinity of the turning points there exist strong density peaks, in which numerous neutrons are produced in collisions of fast tritons with thermal deuterons.

A three-component version of the GDT-based neutron source is distinguished from the two-component one desribed above by additional injection of fast deuterons simultaneously with tritons. In this case the central cell plasma contains two energetic ion components whose densities are similarly peaked near the turning points. As both the components are then of high energy, the D-T reaction rate increases in comparison to the previous case, thereby allowing the injecton energy to be reduced to $\approx$ 100keV. Generally, this reduction might be significant when one considers the technological basis of the neutron source. An injection energy as high as 200keV immediately requires involving the less proven technology based on a negative ion source whereas reduction to 100keV makes it possible to rely upon rather well established positive ion sources.

Previous studies of a mirror-based beam-target neutron source /6,11/ have emphasized that the proven high β (β is ratio of plasma pressure to magnetic field pressure) containment inherent in mirror systems is highly advantageous for testing materials in a fusion environment. Particularly, such a system would satisfy the following basic requirements /4/:

- Providing the same neutron spectrum as that of a fusion reactor.
- Relative simplicity and low both capital and operational costs.
- Reasonable tritium comsumption amounting to a few persents of annual world production.
- Providing the desired fluence of 10-20 MW· yr. in reasonable time. Capabilities to provide the accelerated tests.
- Easy access to testing zone.

Basic GDT-based neutron source parameters are given in Table 1 for both two- as well as three component versions.

Table 1. Neutron source parameters

Parameter	two	three
T_0 beam energy (keV)	240	100
D_0 beam energy (keV)	-	100
T_0 beam power(MW)	20	12.3
D_0 beam power (MW)	-	16.2
Electron temperature	0.6	1
Plasma density (m^{-3})	$2 \cdot 10^{20}$	$1.23 \cdot 10^{20}$
Plasma radius at the	0.06	0.08
Mirror ratio, R_m	20	23.7
Central field (T)	1.25	1.25
Injection angle (deg.)	20	23.3
Maximum neutron flux	3.9	2.1
Power consumption	50	100

2. Main goals and target parameters of HPNS.

During the last decades an extensive plasma-physics database has been generated in magnetic mirror research. Analysis of the data for the parameters relevant to the neutron source, in general, provides rather optimistic predictions regarding its parameters. It should be emphasized that most of the basic physical principles of the source have been already proven experimentally; e.g. MHD and kinetic stability, high beta ($\beta \approx 1$) operation in the mirror cell, quasi-steady-state operation in the beam-target regime have been demonstrated in 2XIIB /9/ and TMX /10/ experiments. These experiments have also confirmed that classical hot ion slowing down scaling /8,11/ is produced when the drift cyclotron loss-cone mode is suppressed by addition of a small amount of Maxwellian plasma. The relevant hot ion density of $\approx 1.5 \cdot 10^{20} m^{-3}$ has also been achieved experimentally /9/. The extension of these results to steady-state operation is considered straightforward.

In contrast to a toroidal system in which it might be a serious problem, in open-ended systems like GDT-based neutron source, the He-ash and heat are removed quite naturally along field lines. An acceptable heat load for divertor plates of a tokamak is considered to be 10-30MW/m^2. This value is about two orders of magnitude higher that the heat load expected at the end-wall plasma dumps in the considered neutron source /4/.

There are several important problems that still need to be solved both theoretically and experimentally. Among them are the accurate self-consistent analysis of MHD-stability which would be modified by the presence of fast drifting ions /12/ and the ballooning effects, whether there is worse anomalous target plasma cross-field transport resulted from a drift wave turbulence, and the effect of the plasma equilibrium from magnetic field imperfections as well as from asymmetry of the neutral beams, etc. Careful study is needed for the radial electric fields effect on the plasma cross-field transport. The issue of vital importance for the whole project is how to achieve the bulk electron temperature as high as 1keV whereas a maximum of 260eV has been obtained as yet /10/. Generally, due to rapid electron thermal loss along magnetic field lines, the electron temperature is limited in open-ended beam-target systems. This condition limits the fast ion energy lifetime and correspondingly the source power efficiency, both of which are proportional to $T_e^{3/2}$. If T_e can be improved, a major upgrade in efficiency arises. To be more realistic in our estimates of the neutron source parameters, we have limited the electron temperature to 10^{-2} of injection energy as was obtained experimentally in /7,9,10/. Thus, our estimates were based on relatively modest assumptions for achieveing interesting plasma parameters for a neutron source. Nevertheless, an intermediate scale experiment is certainly needed to prove the feasibility and guarantee the reliability of the proposed neutron source.

The Hydrogen Prototype (acronym HPNS) is intended to generate a plasma physics database at plasma parameters as close as possible to those expected in the GDT-based neutron source. This mission determined the approach to its design as an experimental facility with sufficiently high flexibility and pulse mode operation using power supplies available at the INP site. Using the results of numerical simulations with the code discribed in /13/, we have estimated the parameters of HPNS which are presented in Table 3. A list of notations used is given in Table 2.

For diagnostic as well as for safety purposes we also have calculated D-D neutron flux from the plasma. Doing these calculations we used the following notations: NEUTR is D-D neutron flux; QLM is neutron power per meter inside the region of maximal density, QNM is neutron power per m^2 of plasma interface inside the same region; QL0 is neutron power per meter in the center, QN0 is neutron power per m^2 in the same position; $\langle\sigma\ v\rangle_{DD}$ - D-D reaction rate calculated at maximum of density, $\langle\sigma\ v\rangle^0_{DD}$is D-D reaction rate at the center of the machine.The results of neutron calculations are presented in Tabl. 4. Here * designates the independent parameters which varied to optimize operational regime.

Table 2.

*WD	injection energy (D-beams)
*PD	trapped neutral beam power
P_{inj}	injected power
P_e	energy loss from electrons due to gas puffing
T_e	electron temperature
T_i	cold ion temperature
U/T_i	MAX of ambipolarpotential over T_i
JI	equivalent current of pellet injection
JD	deuterium current trapped in the plasma
JD0	flux of neutral deuterons hitting the first wall
*L	an effective plasma length
*A	plasma radius at the midplane
*DINJ	diameter of the neutral beam
*TETA	pitch angle of the fast component in the center part of the machine
* H_{max}	magnetic field in mirrors
*K	mirror ratio (H_{max}/H_{max})
KSTOP	mirror ratio in the maximum of plasma density (H/H_{min})
LRI	number of Larmor radii over the plasma radius for the cold ions
LRD	number of "transverse" Larmor radii over the plasma radius for fast deuterons
RD	ratio of the NB-beam penetration length to plasma radius in the injection region
n_e	electron density in the center
n_i	cold ion densityin the center
n_D	density of fast deuteron in the center
n_{IM}	cold ion density in maxima of density of fast ions
n_{DM}	maximal density of fast deuterons
N_{IO}	density of the cold neutrals averaged over the entire plasma volume normalized to N_e
ND0	density of the deuterium neutrals averaged over the entire plasma volume normalized to N_e
CED	amount of the energy transferred to electrons from the trapped deuterons
CID	amount of the energy transferred to cold ions from the trapped deuterons
CCD	amount of the energy lost through the loss-cone
C0D	amount of energy lost via neutral outflux
BETN	$\beta_\perp$ in the center
BETL	$\beta_\parallel$ in the center
TAUI	ion lifetime which equals to $TAUI_{gdl} + TAUI_{kin}$
TAUED	time of ion-electron interaction for deuterons

Table 3. HPNS parameters

parameter\version	1	2	3	4	5
*WD, kV	20.0	30.0	40.0	50.0	60.0
*PD ,MW	5.0	5.0	5.0	5.0	5.0
P_{inj} , MW	7.2	7.8	8.3	8.6	9.1
P_e ,MW	-2.83	-2.78	-2.83	-2.93	-2.99
*T_e , keV	0.20	0.30	0.40	0.50	0.60
T_i ,keV	0.20	0.30	0.40	0.50	0.60
U/TI	0.30	0.31	0.31	0.30	0.30
JI, A	110.40	71.60	57.10	51.60	46.30
JD, A	250.0	166.7	125.0	100.0	83.3
JD0, A	113.4	84.4	60.9	42.5	32.1
*L, m	5.0	5.0	5.0	5.0	5.0
*A,cm	10.0	10.0	10.0	10.0	10.0
*DINJ, cm	14.0	14.0	14.0	14.0	14.0
*TETA	40.0	40.0	40.0	40.0	40.0
*H_{max} , T	18	18	18	18	18
*K	10.0	10.0	10.0	10.0	10.0
KSTOP	2.24	2.24	2.24	2.24	2.24
LRI	62.3	50.9	44.1	39.4	36.0
LRD	9.7	7.9	6.9	6.1	5.6
RD	1.35	1.57	1.74	1.88	2.04
n_e , $10^{14}/cm^3$	0.41	0.45	0.49	0.54	0.57
n_i ,$10^{14}/cm^3$	0.20	0.30	0.40	0.50	0.60
n_d , $10^{14}/cm^3$	0.37	0.40	0.44	0.48	0.51
n_{im} , $10^{14}/cm^3$	0.03	0.03	0.04	0.04	0.04
n_{dm}, $10^{14}/cm^3$	0.83	0.92	1.00	1.06	1.11
NI0/n_e	$2.5\ 10^{-5}$	$1.4\ 10^{-6}$	$8.6\ 10^{-6}$	$5.4\ 10^{-6}$	$3.6\ 10^{-6}$
ND0/n_e	$3.0\ 10^{-4}$	$1.6\ 10^{-4}$	$1.0\ 10^{-4}$	$6.8\ 10^{-5}$	$5.1\ 10^{-5}$
BETN	0.02	0.04	0.05	0.07	0.09
BETL	0.04	0.08	0.11	0.14	0.18
CED	0.62	0.61	0.62	0.65	0.66
CID	0.02	0.02	0.02	0.02	0.02
CCD	0.12	0.12	0.12	0.13	0.13
C0D	0.24	0.26	0.24	0.21	0.18
TAUI, s	$9.5\ 10^{-4}$	$1.6\ 10^{-3}$	$2.2\ 10^{-3}$	$2.6\ 10^{-3}$	$3.1\ 10^{-3}$
TAUED, s	$5.7\ 10^{-3}$	$9.7\ 10^{-3}$	$1.4\ 10^{-2}$	$1.8\ 10^{-2}$	$2.2\ 10^{-2}$

Table 4. HPNS neutronics

NEUTR, s^{-1}	$1.6\ 10^{14}$	$6.2\ 10^{14}$	$1.5\ 10^{14}$	$3.0\ 10^{15}$	$4.2\ 10^{15}$
QNM, MW/m^2	$2.8\ 10^{-5}$	$9.9\ 10^{-5}$	$2.3\ 10^{-4}$	$4.5\ 10^{-4}$	$5.9\ 10^{-4}$
QLM, MW/m	$1.2\ 10^{-5}$	$4.1\ 10^{-5}$	$9.7\ 10^{-5}$	$1.9\ 10^{-4}$	$2.5\ 10^{-4}$
QN0, MW/m^2	$4.1\ 10^{-6}$	$1.5\ 10^{-5}$	$3.7\ 10^{-5}$	7.7 10-5	$1.1\ 10^{-4}$
QL0, MW/m	$2.5\ 10^{-6}$	$9.4\ 10^{-6}$	$2.3\ 10^{-5}$	$4.8\ 10^{-5}$	$6.9\ 10^{-5}$
$\langle\sigma v\rangle_{DD}$, cm^3/s	$3.1\ 10^{-19}$	$8.7\ 10^{-19}$	$1.7\ 10^{-18}$	$3.0\ 10^{-18}$	$3.5\ 10^{-18}$
$\langle\sigma v\rangle^0_{DD}$, cm^3/s	$1.4\ 10^{-19}$	$4.6\ 10^{-19}$	$9.5\ 10^{-19}$	$1.6\ 10^{-18}$	$2.0\ 10^{-18}$

3. General layout

The HPNS facility, as shown in Fig.1, has a completely axisymmetric configuration, and the central cell composed of the central section 2.4m in diameter and the two side sections 0.75m in diameter with anchor cells 2.6m in diameter on both sides of the central cell. Its position inside the experimental bunker is shown on Fig.2. It has an axial length of about 16m, and the total volume of the vacuum vessel of $35m^3$ excluding the NBI tanks. The anchor cells are used to provide MHD stability for the entire system and have a Min-B configuration. The mirror ratio of the central cell can be varied by energizing the mirror coil inserts with independent power supplies. The central cell has a mirror-to-mirror length of 10m.

The helium cryopump system consists of toroidal cryopanels installed inside the neutral beam line and is operated at the temperature of $4.2^{\circ}K$, and cryopumps installed on the central cell as well as on the end cell vacuum chambers. The pumping speed at the NBI tanks is $4\text{-}5\cdot10^5$ l/s.

Plasma start-up in HPNS will be carried out by injecting a plasma along the field line from an end. Then the injected cold target plasma is heated up and sustained by a combination of neutral beam heating and gas puffing and/or injection of low energy ($\approx$100-200eV) neutrals. A pulsed ring-shape plasma gun has been developed to produce sufficiently dense hydrogen plasma with high ionization degree and small impurities. The gun has a coaxial configuration with annular anode and cathode. More details on plasma build up system are given in Section 4.4.

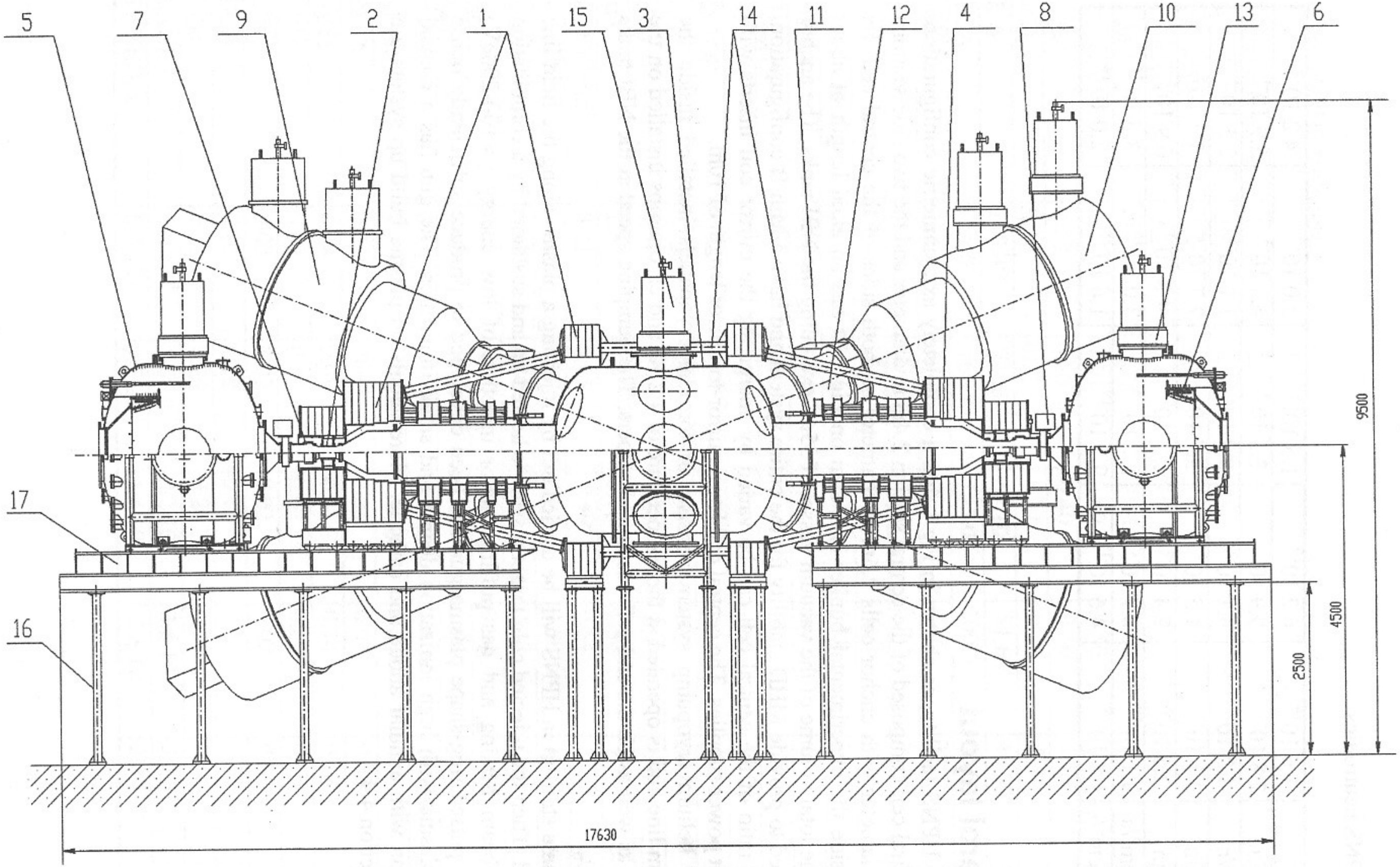

Fig.1 HPNS general layout.

1.Central cell coils; 2.Mirror inserts; 3.Central cell vacuum chamber; 4.Side chambers; 5.Ribbbed surface; 6.Plasma dump; 7.Bellow; 8.Gate valve;

9.Injector tank; 10 Neutralizer chamber; 11.750mm gate valve; 12.Compensating bellow; 13.Gate valve; 14.Mechanical structure; 15.BKN-7000 cryopump; 16.Supports; 17. Rails.

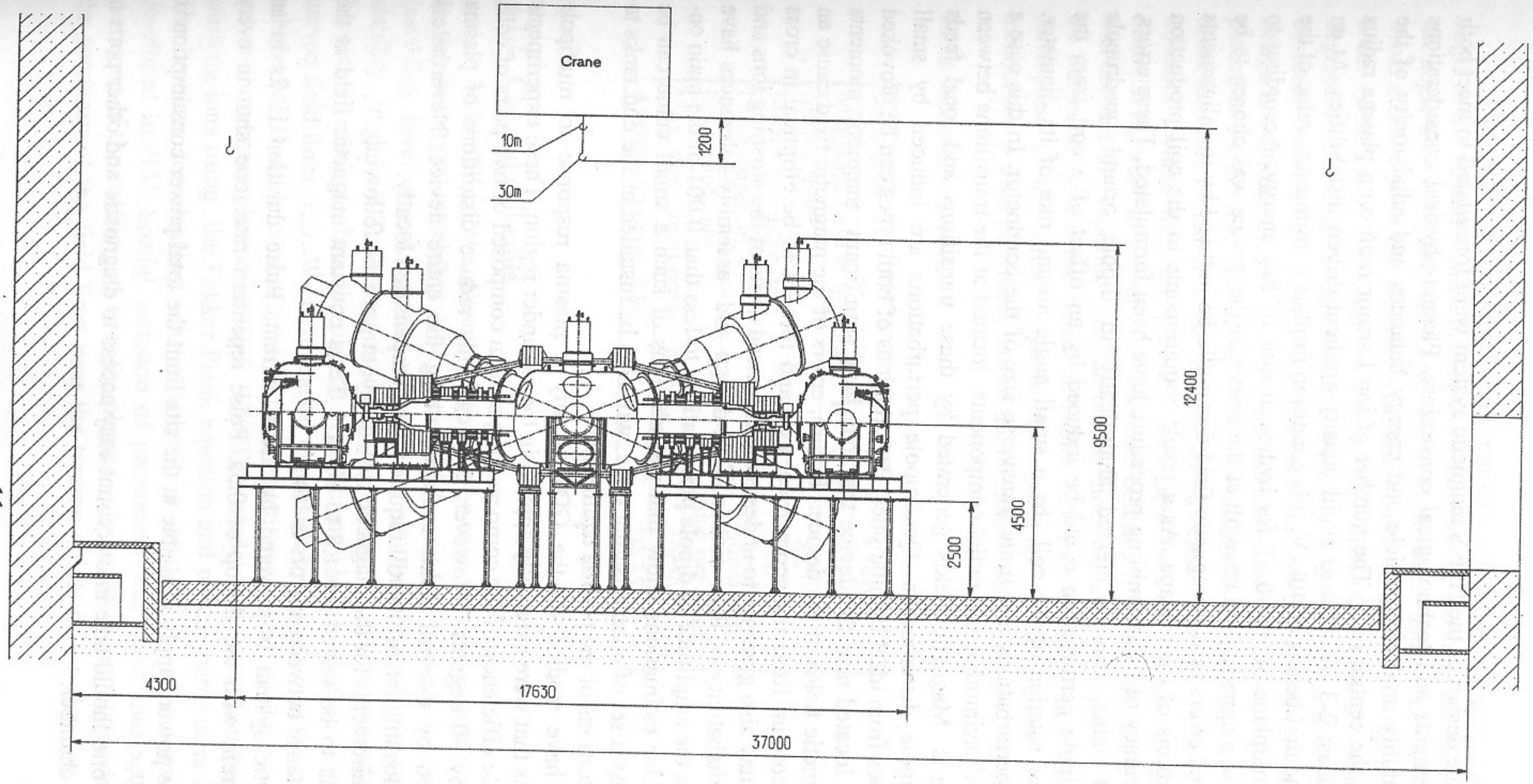

Fig.2 HPNS view inside the experimental bunker.

4. The main subsystems of HPNS

4.1 Magnets

Initial data for the design of the HPNS magnetic system were formulated to meet both plasma physics requirements and technological constraints. Plasma-physical considerations involved the MHD-stability analysis, particle and energy balances and adiabaticity of the sloshing ion motion in the central cell. The number of ion Larmor radii on a plasma radius was required to be at least 2-3 in order to avoid density-gradient-driven instabilities. At an energy of the HPNS's neutral beams of 40keV, this condition implies a minimum value of the magnetic field at the midplane of 0.4-0.6T for hydrogen ions of full energy. According to these considerations, the magnetic field strength at the center of the device was chosen to be 1T. We have considered errors of the magnetic field that could be induced by misalignments of the coils and distortions of their shape. As a result, requirements to the coil production technology and the accuracy of its assembling procedure have been formulated. These errors, as being of a small value, can be treated analytically in dipole or/and quadrupole approximation. The dipole perturbation could be induced by an offset of a coil from the geometrical axis and/or rotation of the coil by a small angle around one of its diameter. Another cause of the perturbations is a finite transverse size of the conductor. In this case a current has to have both azimuthal and radial components located at the transitions between different layers of turns. Magnetic fields generated by these transitions and local feeds contribute also to dipole disturbances. Quadrupole perturbations are induced by small deviations of coil shapes from ideal circular ones. Perturbations of both types can be provoked also by metallic parts located near the device that may have significant magnetic moments induced by stray magnetic fields of the device. In turn, errors of the magnetic field cause an offset of the plasma column from the geometrical axis and force it to be elliptical in cross section. These errors may also give rise to undesirable enhanced drifts of the sloshing ions and provoke the lost of adiabaticity of their motion. Coil design and assembly tolerances have been chosen to reduce the amplitude of dipole perturbations to less than 0.001 of the main on-axis magnetic field. Our estimations show that perturbations of such a small value can be neglected. Nevertheless a set of compensating coils will also be installed at the end tanks to reduce further the distortions of the plasma equilibrium.

Recently we have studied on the GDT facility a plasma response to multipole magnetic perturbations that were externally applied in the expander region. These experiments have shown reasonable efficiency of the compensating system composed of two pairs of coils azimuthally shifted by 90 degrees. However, they can only reduce distortions of plasma equilibrium controlled by external fields averaged along the entire device. Nevertheless perturbations of the sloshing ion orbits still require to be compensated locally.

The main requirements for the magnetic system layout were the following:

1. The mirror ratio is to be varied from 8 to 20 at 1 Tesla constant magnetic field at the midplane. The distance between mirrors is 10m.
2. The main magnetic system is powered by 25kA current. Pulse duration is 2s in an equivalent dc-current with the flattop of 0.5s. Pulse repetition rate: one shot in every 20min.
3. Capabilities of the power supply available at the site limit the total power consumption of the coils to 40MW.
4. In the coil set-up one should take into account easy access to diagnostic and other ports in the main vacuum chamber.

5. The coils should be unified in size and production technology and use available copper conductors.

One of the parameters that substantially affect the magnetic coil design is the injection angle of the neutral beams. In order to maximize the sloshing ion density at the turning points the angle should be as small as possible. On the other hand, it cannot be too small in order to avoid a decrease in the sloshing ion lifetime due to an increased scattering rate into the loss cone. Technically, it also turns out to be very difficult to obtain injection angles less than 30 degrees. In this case the gap between the coils, where the neutral beams are passing through, becomes inadmissibly large. As a compromise between the above mentioned physical and design limitations, the injection angle was taken to be 30 degrees. Figure 1 shows the general pattern of the device. As can be seen from this cut-away drawing, the device has four neutral beam injectors aimed at its center. Untrapped beams enter the dumps located opposite to the injectors where they are partially implanted into end plates or reflected as low energy neutrals. In order to prevent the scattered neutrals from coming back into the central cell, it was decided to evaporate titanium on the inner walls of the dumps. The main parameters of the magnetic system are listed in Tables 5,6. Indicated in parentheses are the values that correspond to the initial stage of the operation of the facility when only the existing transformer is used providing half of the nominal electric power to the coils.

Table 5 Central cell coils

Parameter	Value
Magnetic field at midplane, T	1 (0.7)
Mirror ratio	8-20
Mirror to mirror, m	10
Pulse duration, s	2 (equivalent)
Repetition rate	1 pulse per 20min
Max. consumed power, MW	40(20)
Averaged power, kW	70(35)

4.1.1 Central cell coils

As is well known, plasma confined in an axisymmetric magnetic field can be subjected to the flute-type instability /14/. To avoid tremendous plasma losses accompanying the instability development, pressure-weighted curvature of the field lines should be favorable for stability. In the GDT, this requirement can be met due to contributions from the regions beyond the mirrors where the plasma of sufficiently high pressure is flowing along favorably curved field lines /1,2/. We have started the design by optimizing the magnetic field lines to achieve MHD stable confinement. In the simulations we have used the mathematical model of a two-component plasma in GDT /12/. This model calculates distribution functions of the sloshing ions using the Fokker-Plank equation and plasma parameters inside the expanders. The problem for sloshing ions is solved by making use of a semi-analytical approach developed in /13/. Spatial variation of parameters was taken into account by appropriate averaging of the coefficients over the plasma volume. By using this model we have optimized the geometry of the field lines near the turning points of the sloshing ions to reduce their

unfavorable contribution to stability. The plasma inside the expander was simulated using adiabatic and isothermal approximations which can be applied at different electron temperatures. The model also takes into account limitations on maximum allowable β value, the validity of the paraxial limit in current points on a line, the ratio between local curvature radius and ion Larmor radius, etc. Near the midplane, where the neutral beams are trapped, the magnetic field should be closely homogeneous to avoid enhanced initial spread of the sloshing ions over the pitch angles. Given these limitations we have recalculated about 10 different versions of the magnetic system. Its final version is shown in Fig.3. Design parameters of the coils are given in Table 6 which includes only half of them because the set is symmetric with respect to the trap center.

Table 6 Parameters of the coils

Coil number	z-pos.	r	Δz	Δr	n	N	NI
1	120.25	135.00	51.50	46.70	5	180	2250.00
2	188.00	48.00	20.60	5.10	2	8	200.00
3	225.00	48.00	10.30	23.40	1	18	450.00
4	257.00	48.00	10.30	23.40	1	18	450.00
5	300.00	48.00	20.60	23.40	2	36	900.00
6	343.00	48.00	30.90	23.40	3	54	1360.00
7	423.70	42.50	82.40	59.00	8	292	3650.00
8	498.00	24.50	61.80	41.60	6	192	4800.00
9	490.00	9.50	14.60	10.50	1	180	3600.00
10	810.00	80.00	10.30	7.60	1	6	-150.00

Here z is a distance from midplane to coil center; r is an inner radius of the coil; $\Delta z \times \Delta r$ is the coil cross-section, n-number of sections per coil; N is the number of turns; NI is the total current in coil, kA. All dimensions are given in centimeters. The 7th coil consists of 8 sections which were previously used as a part of the magnetic system of the PSP-2 facility /15/. They are made of copper conductors of 25mm x 50 mm in cross-section with a hole of 15mm in diameter and 42mm x 50mm cross-section with a 20mm hole. These coils generate magnetic fields with high axial symmetry almost all over their inner diameters because of a special design of transition windings between the layers /15/. As it was already mentioned, these transitions may give dipole perturbations when a finite thickness of conductors is taken into account. Coil 8 is of the same design. By now the production of the coils has been started in the INP machine shop. All of them (except coil 9 whose design is given in the next section) consist of sections of the same design and their manufacturing technology differs only due to difference in diameters and numbers of turns. Thus the magnetic system (excepting 7 and 9 coils) consists of only 5 standardized sizes of the sections which are used for assembling the coils. The largest coils 1 with an outer diameter of 3.7m consist of 5 sections and each of them is mounted on fixed supports. The other coils are installed on movable carts and are aligned with respect to the first one. The axial position of coils is determined by the spacers/stretchings which support the corresponding component of the ponderomotive forces. All the coils (except coils 9 having separate power supplies) are connected in series. The coils 1 and 7 are incorporated into the common circuit being preliminary connected in parallel by pairs, so that their windings are carrying half the total current. Two rectifying units each of nominal power 20MW (voltage - 800V, nominal current

- 25kA) are to be used to energize the magnets. One of them in the near future will be available and up to now it is used at the PSP-2 facility. During the single pulse the coils 1 and 7 are heated by 1.4°C and the remaining coils except for 9 - by 5.7°C. The mean power consumed by the coils is 67kW. We planned to remove the heat by distilled water using available heat-exchanger of 1MW power. This heat-exchanger has enough capacity to keep the temperature of the coils close to required values. We also planned to switch on the cooling system during the baking of the vacuum chamber for outgassing. In this regime it is used to prevent the overheating of the coils insulation.

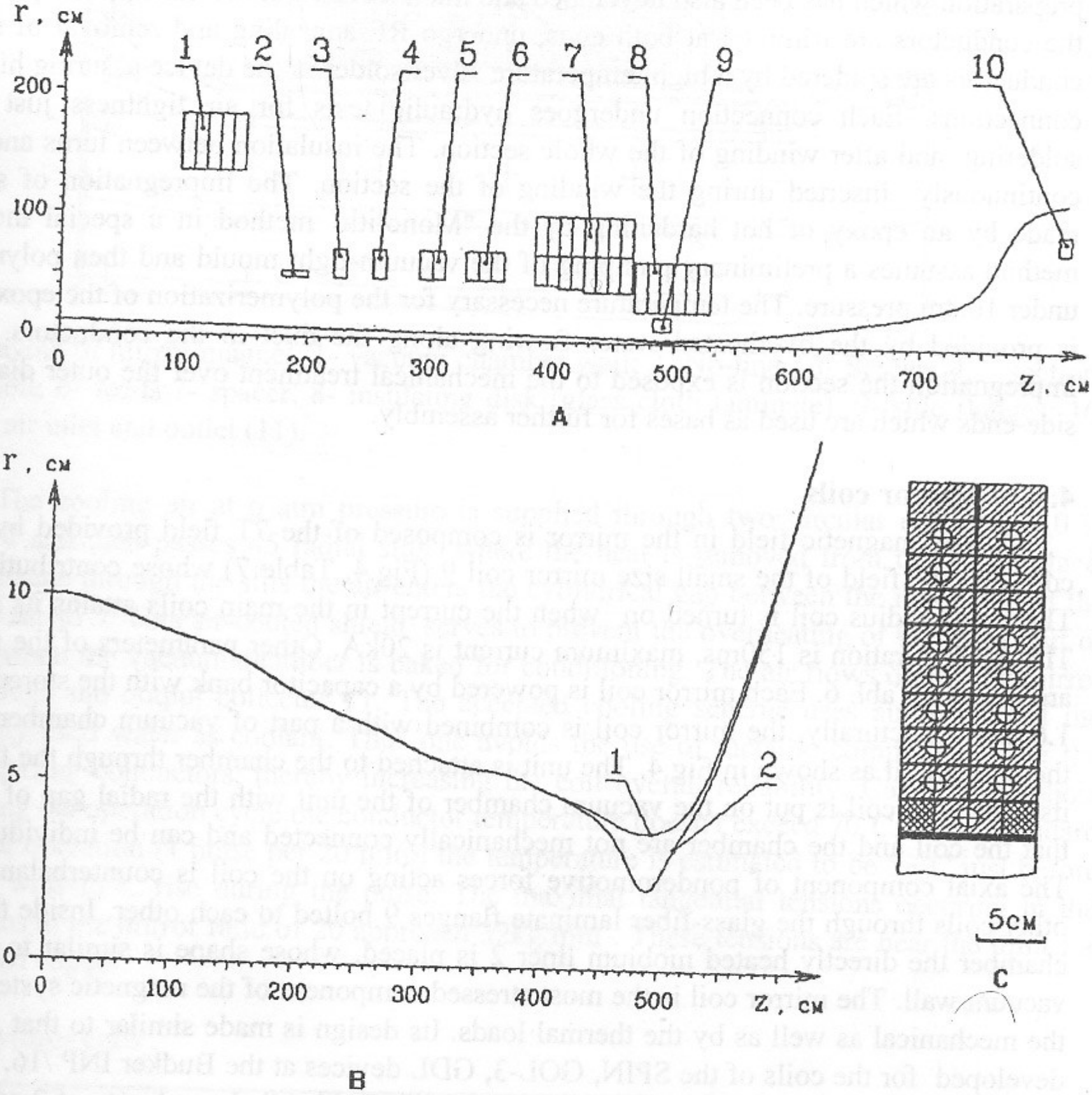

Fig.3 Magnet system of HPNS
A.- layout of the coils and on axis magnetic field; B - magnetic field lines started from 10cm radius at midplane: 1 - coil 9 is not energized, 2 - coil 9 is energized; C - cross-section of a coil.

A section of a coil (Fig.3) consists of two flat spirals wound with the copper conductor of 25mm x 50mm in cross-section with a hole of 15 mm in diameter. The insulation between the turns and layers is made of fiberglass laminate impregnated with epoxy. The standard section with insulation is 103mm thick. The conductor's ends are connected with the end plates which have holes for connection with the water pipes.

The technological line has been developed and manufactured in the machine shop for manufacturing the coil sections. The main components of the line are the specially developed low-turn (with a large torsional moment) machine, a tightening device, a device for airtight soldering of the conductors, a milling machine for preparing the conductor's ends for soldering. Before winding the coils, the conductors pass through the line of preliminary preparation which has been also developed and manufactured at the machine shop. In this line the conductors are trimmed at both ends, undergo RF annealing and removal of scale. The conductors are soldered by a high temperature silver solder in the device assuring high quality connections. Each connection undergoes hydraulic tests for air tightness just after the soldering and after winding of the whole section. The insulation between turns and layers is continuously inserted during the winding of the section. The impregnation of sections is made by an epoxy of hot hardening by the "Monolith" method in a special mould. This method assumes a preliminary pumping of the vacuum-tight mould and then polymerization under 10atm pressure. The temperature necessary for the polymerization of the epoxy (120°C) is provided by the overheated water flowing along the duct in the conductors. After the impregnation the section is exposed to the mechanical treatment over the outer diameter and side-ends which are used as bases for further assembly.

4.1.2 Mirror coils

The magnetic field in the mirror is composed of the 7T field provided by the main coils and the field of the small size mirror coil 9 (Fig.4, Table 7) whose contribution is 13T. This small radius coil is turned on when the current in the main coils attains its maximum. The pulse duration is 150ms, maximum current is 20kA. Other parameters of the mirror coil are given in Tabl. 6. Each mirror coil is powered by a capacitor bank with the stored energy of 1.65MJ. Structurally, the mirror coil is combined with a part of vacuum chamber providing the mirror unit as shown in Fig.4. The unit is attached to the chamber through the flanges 1 at its ends. The coil is put on the vacuum chamber of the unit with the radial gap of 1.75cm so that the coil and the chamber are not mechanically connected and can be individually fixed. The axial component of ponderomotive forces acting on the coil is counterbalanced by the other coils through the glass-fiber laminate flanges 9 bolted to each other. Inside the vacuum chamber the directly heated niobium liner 2 is placed, whose shape is similar to that of the vacuum wall. The mirror coil is the most stressed component of the magnetic system by both, the mechanical as well as by the thermal loads. Its design is made similar to that previously developed for the coils of the SPIN, GOL-3, GDL devices at the Budker INP /16,17,18/. The coil itself consists of two sections 4 and 5 made of a cold-rolled conductor of 2 mm x 70mm in cross-section. The sections are connected by the common inner loop. The total number of turns in the coil is 180. The sections are isolated between each other by 1 mm thick fiber-glass spacer. The insulation between turns is two layers of cable paper 0.08 mm thick. From its outside each section is rimmed by a fiber-glass band 7. After winding the coil is impregnated by epoxy with the use of the same technology as the central cell coils. The conductor, the coil is made of, is sand blasted before winding to improve the adhesion of the epoxy. The coil is air-cooled between the shots from its side surfaces.

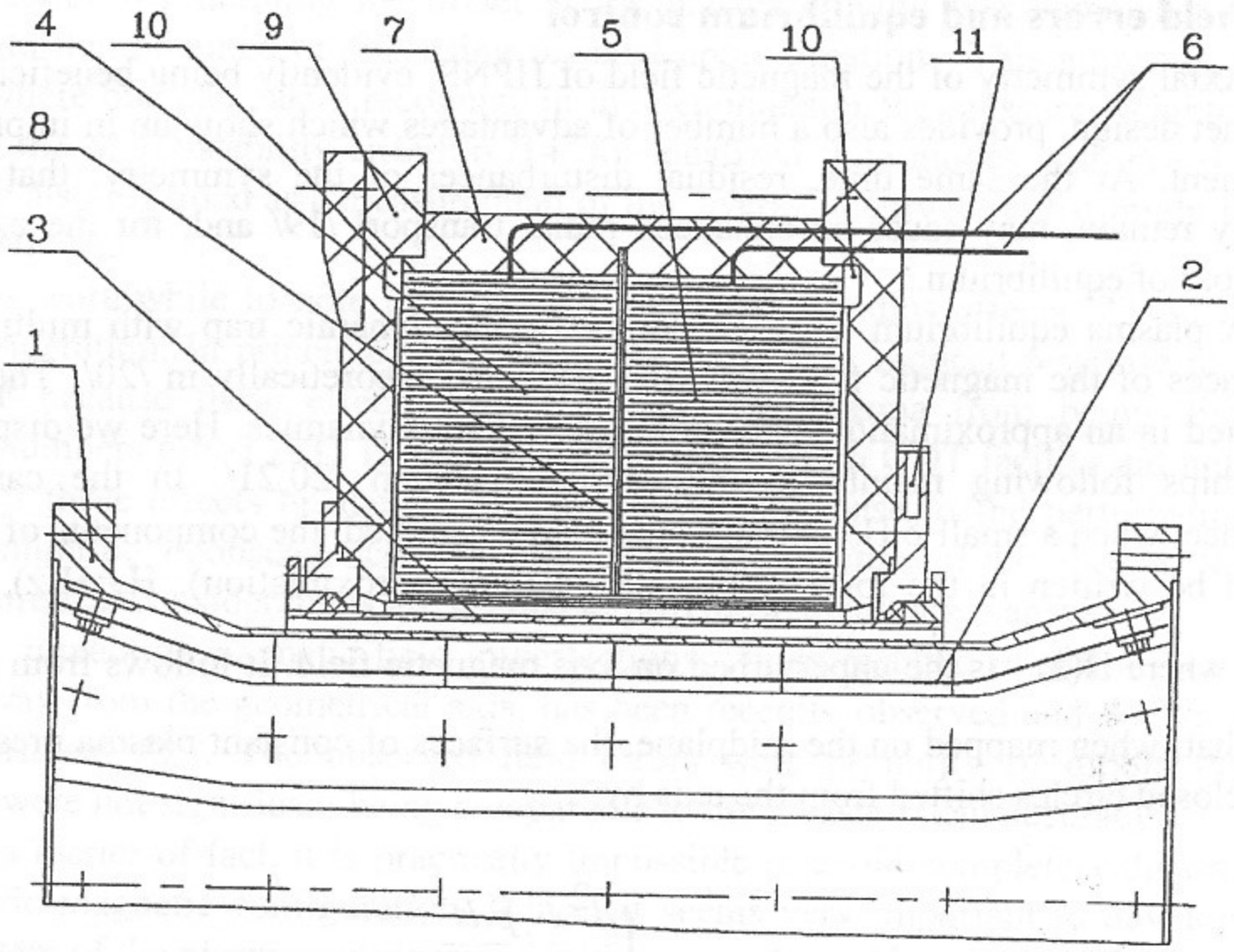

Fig.4 Layout of mirror magnet: 1- vacuum chamber wall; 2- Nb-liner; 3- Screen; 4,5- sections of the coil; 6- feeds;7- spacer, 8- insulating disk (glass cloth laminate); 9- side flanges; 10- cooling air inlet and outlet (11).

The cooling air at 6 atm pressure is supplied through two circular collectors 10 in flanges 9 and then passes 45 radial slits where the heat is removed from the coil surface. After passage through the slits the air enters the cylindrical gap between the inner side of the coil and shield 3. This air-cooled shield serves to prevent the overheating of the inner part of the coil when the vacuum chamber is baked for conditioning. The air flows out of the mirror unit through the output collector 11. The accepted cooling scheme uses air instead of the commonly used water as coolant. Thus one avoids the use of metallic components near the current-carring conductors, thereby increasing the coil overall reliability. Calculations show that during the operation cycle the conductor temperature doesn't exceed 70°C. In the standard regime of operation (1 pulse per 20 min.) the temperature is estimated to be 53°C just before the shot with 17°C rise during the pulse. The maximal tangential tensions occuring in the coil's turns at the mirror ratio of 20 approach 32kg/mm^2. These tensions are near the limit for cold-rolled copper.

Table 7 Mirror coils

Parameter	Value
On axis magnetic field, T	13
Max. current, kA	20
Max. applied voltage, kV	6
Pulse duration, s	0.15
Stored energy, MJ	1.65(in each coil)
Conductor cross-section, mm x mm	2x70
Number of turns	180

4.1.3 Field errors and equilibrium control

Axial symmetry of the magnetic field of HPNS, evidently being beneficial in itself to the magnet design, provides also a number of advantages which show up in improved plasma confinement. At the same time, residual disturbances of the symmetry, that nevertheless inevitably remain, may cause an enhanced radial transport /19/ and, for the extreme cases, even in loss of equilibrium.

A plasma equilibrium in an axisymmetric gas-dynamic trap with multipole external disturbances of the magnetic field was first discussed theoretically in /20/. The equilibrium was treated in an approximation of ideal magneto-hydrodynamics. Here we display the main relationships following mainly to the results given in /20,21/. In the case of dipole disturbance, when a small $\delta H_x(z)$ transverse field is applied, the components of the magnetic field can be written in the form (using a long thin approximation): $H_z=H(z)$, $H_x=\delta H_x(z)-\frac{x}{2}H'(z)$, where H(z) - is the unperturbed on-axis magnetic field. It follows from the results of /20,21/ that, when mapped on the midplane, the surfaces of constant plasma pressure are then to be enclosed circles shifted from the axis by:

$$\Delta x = \frac{1}{\sqrt{H_0}} \cdot \frac{\int \frac{d^2x}{dz^2} \frac{\tilde{p}ds}{H^{3/2}}}{\int \frac{\tilde{p}\kappa ds}{H^2 r}} \qquad 4.1$$

Here $\tilde{P} = P_\perp + P_\parallel$ is a sum of transverse and longitudinal pressures, function $\delta x = R(z)^{1/2} \int_{-l}^{l} R(z)^{1/2} \frac{\delta H_x}{H(z)} dz$, where the integrand comprises corresponding component of the magnetic field perturbation- δH_x, and $\frac{d^2\delta x}{dz^2}$ is an additional field line curvature connected with the existance of disturbance.

If a quadrupole disturbance of the form $\delta H_x = -2b(z)x\,; \delta H_y = +2b(z)y\,,$ $\delta H_z = -(x^2 - y^2)\frac{db}{dz}$ is applied, it makes the surfaces of constant pressure take the form of ellipsoids with ellipticity of:

$$\int \frac{dz \cdot \tilde{p} R^{1/2} E^{-1/2}}{H^2} \cdot \frac{d^2 R^{-1/2} E^{1/2}}{dz^2} \Big/ \int \frac{dz \cdot \tilde{p}(RE)^{1/2}}{H^2} \cdot \frac{d^2 (RE)^{-1/2}}{dz^2} \qquad 4.2$$

where $E(z) = \exp(4 \int_0^z \frac{b(z)dz}{H(z)})$, R is a current mirror ratio.

Integration in 4.1, 4.2 is performed along the entire trap between the end walls which is considered to be insulating.

Equation 4.1 defining the offset of the plasma column was somewhat rewritten as compared to that obtained in /20/ using paraxial approximation. This allows to reduce it to the form where one can easily recognize in the denominator the pressure weighted curvature that enters the MHD-stability criterion /14/ for localized flute modes with m>>1. Thus such data can be also regarded as a measurement of the averaged curvature that might be attractive for diagnostic use.

It is worthwhile to note the role of finite Larmor radius effects /22/ in the problem under consideration. In principle, one could expect strongly reduced response to quadrupole disturbance because these effects could prevent the plasma from being distorted with azimuthal numbers m>>1 /23/. However, our experiments on GDT facility did not reveal any influence of these effects on the plasma equilibrium response to the perturbations. In our case, this might be a consequence of the rather low temperature of the plasma. Nevertheless, further theoretical considerations are needed to provide a quantitative answer.

The impact of magnetic field imperfections, which resulted in shifting of the plasma position away from the geometrical axis, has been recently observed and documented in the GDT experiment /25/. The observed field errors were primarily of dipole type. Higher harmonics were not significant being comparable to the measurement accuracy.

As a matter of fact, it is practically impossible to avoid completely distortions of the axisymmetric magnetic configuration. Hence, it seems very important to develop a reliable control system of the plasma equilibrium position as well as of ist shape, which will be able to reduce these distortions to an acceptable level. Furthermore, this system, if complemented by a proper feed back loop could be capable for stabilizing large scale flute perturbations.

Specifically, in HPNS the plasma equilibrium will be controlled by using the coils that produce small transverse magnetic fields in the regions of the plasma expansion beyond the mirrors. As it was first mentioned in /20/, because of the fact that the main magnetic field here is quite small, the external field applied in these regions could alter the equilibrium to the maximum possible degree.

4.1.4 Application of controlled disturbances

Having developed the relevant theory, it is necessary to perform experimental tests in order to quantify some parameters in theory which define the absolute value of the plasma response to disturbance. In the case of MHD-approach used this critical parameter is an upper limit of integration in 4.1, 4.2 which corresponds to near-end-wall spatial points inside the expander tanks. This limit was fixed by adjusting the measured response to its prediction from 4.1, 4.2 .

In our experiments on GDT facility, the dipole perturbations in the expander were produced by a pair of coils with inner radius of 0.84m installed at the distance between them of 2.4m. The magnetic field generated by the coils was practically homogeneous over the expander region occupied by the plasma. Fig.5 shows the shifts of the plasma centroid, measured from its undisturbed equilibrium position, as a function of transverse field amplitudes in the expander.

Quadrupole perturbations in the expander were generated by two pairs of coils of 0.5m in diameter. The currents in opposite coils in each pairs were opposite to generate the additional field of the quadrupole symmetry. In accordance with the conventional approach, we characterized the on-axis amplitude of the perturbation by the quadrupole parameter b(z) appearing in the expression for the disturbed scalar potential $\delta\varphi = (x^2 - y^2)b(z)$.

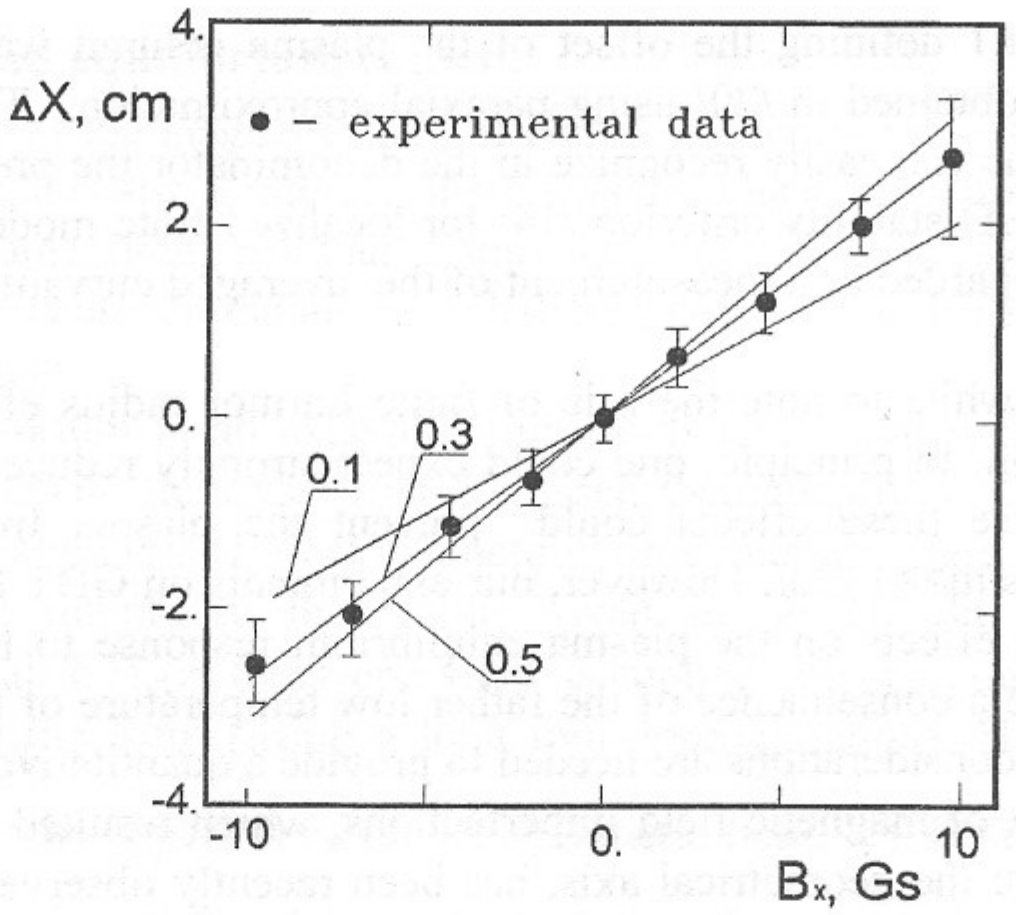

Fig.5 Plasma offset vs amplitude of dipole disturbance

Due to relatively small radius of the disturbing coils, this parameter significantly changed over the expander. Resulted ellipticity of the plasma column was measured by a linear array of the Langmiur probes located inside the central cell and by RF-interferometer (λ =8mm) which measured the linear plasma density along the diameter. The interferometer was situated just beyond the mirror throat in the expander. To deduce the ellipticity from the interferometric data, we have used the values of linear plasma density measured along the perpendicular diameters for subsequent shots in which the currents in the disturbing coils was changed so as one would expect 90° rotation of the ellipsoid around the z-axis. Fig.6 shows the measured ellipticity as a function of value of b(z) taken in the z-position of the center of the disturbing coils.

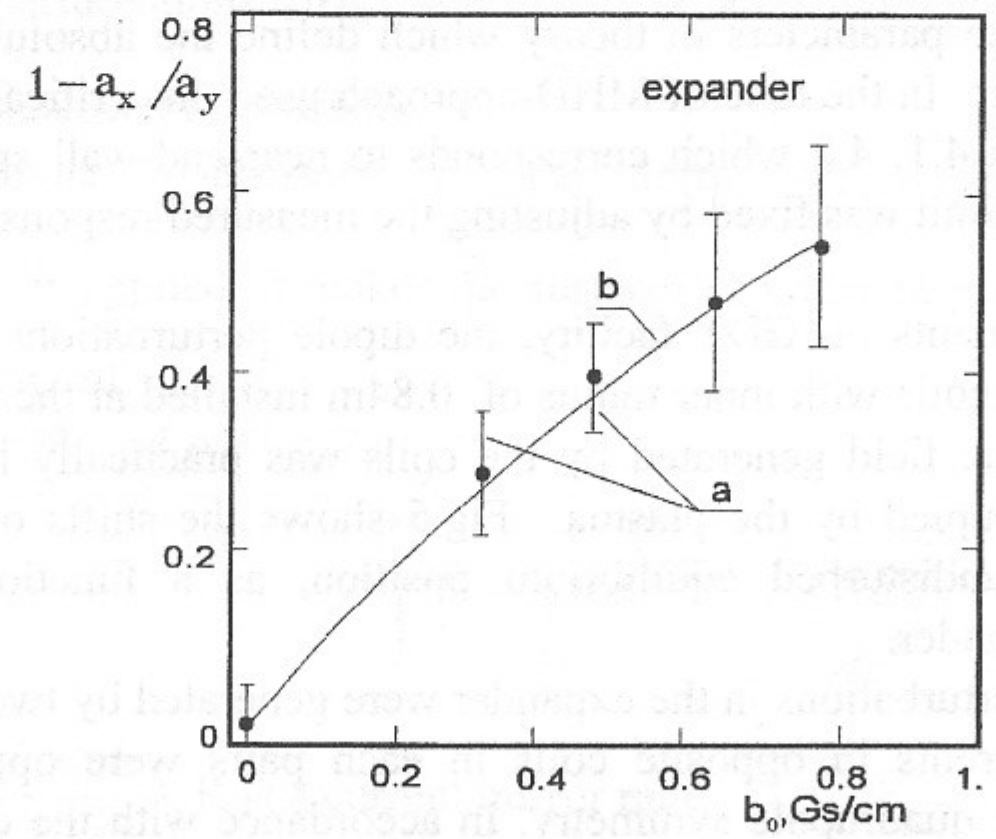

Fig.6 Plasma ellipticity vs amplitude of quadrupole disturbance:
a -- experimental data; b -- calculated for the adiabatic regime of flow and $\kappa\rho_{crit}$ =0.3

The majority of the data were taken when the magnetic field in the end tank was of the expander's configuration. During these experiments, the coils set that provided cusp configuration inside the end tank has been installed /26/. Thus we were able to choose the cusp or expander configuration for use in certain series of shots by reconnecting outer and inner coils of the end tank. The plasma inside the cusp was fed by the collisional losses from the central cell.

A distinct feature of the cusp-anchored gas-dynamic trap is the singularity of a specific volume of the flux tubes $\int dl/H$ near the axis. A theory that relevant to this case /27/ deduces the equilibrium response which is quite different as compare to that for trap with expander end cell. The measured ellipticity vs amplitude of the quadrupole disturbance in the cusp is presented in Fig.7.

The data also show reasonable agreement with the MHD plasma model over a wide range of the amplitudes of the disturbances.

Using these data we have designed a equilibrium control system for HPNS. Similar to that used in GDT-experiment it comprises two pairs of 1m radius coils located on the end tank. These coils will be energetized from the power supply feeding the central cell coils.

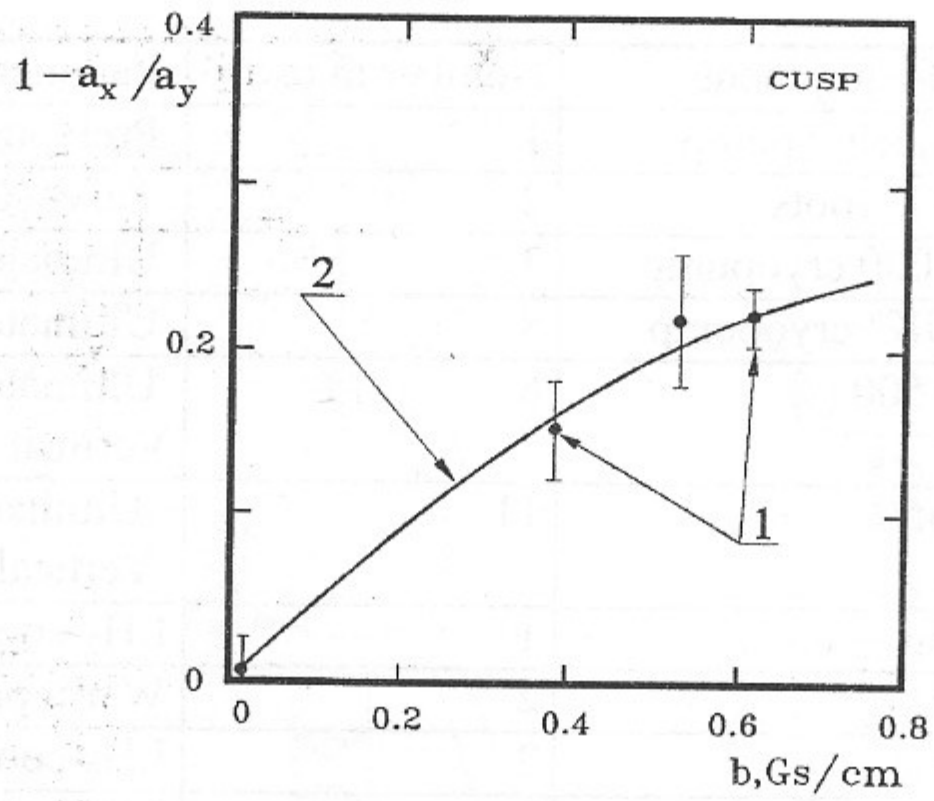

Fig.7 Plasma ellipticity vs amplitude of quadrupole disturbance:
1 - experimental data; 2 - calculated curve.

4.2 Vacuum system

The Hydrogen Propotype vacuum chamber consists of three main chambers: a central cell chamber confining the main plasma, and anchor cells attached to both sides of the central cell. Each of these has an independent vacuum system.The vacuum chamber is shown in Fig.8. The central cell volume is $15m^3$ and in each of the two end tanks it is of $10m^3$.

The energy balance of the central cell plasma is strongly affected by secondary particles released from the first wall under bombardment of charge exchange neutrals. If the recycling coefficient exceeds unity the plasma parameters may significantly degrade. Existence of many monolayers of absorbed gas on the first wall surface immediately provides high recycling coefficients which can not be admitted. In order to prevent the monolayers creation between the shots ($\approx$100s time), the vacuum system was developed to achieve a base pressure less than 10^{-8}Torr in the central cell of the device. This involves the necessity of periodically heating the chamber up to at least 150-200°C for wall conditioning as well as the use of metal seals. Vacuum equipment are specified in Table 8.

Table 8 Specifications of vacuum equipment

	Type of equipment	Number in use	Parameters / Functions
NI1	VN-6 mech. pump	1	Prel. pumping to 10-10^{-2}Torr
NI2,3	AVR-150 roots	2	Turvovacs exhaust 10^{-3}Torr
NK1..3	BKN-7000 cryopump	3	Ultimate vacuum 10^{-6}Torr
NK10..17	"BUBLIK" cryopump	8	Ultimate vacuum 10^{-6}Torr
NR1..6	TMN-1500	6	Ultimate vacuum 10^{-6}Torr Vertical turbopump
NR10..20	TMN-450	11	Ultimate vacuum 10^{-6}Torr Vertical turbopump
NS1	Ti-pump	1	LH_2-cooled
NS2..3	Ti-pump	2	Warm panels
BS1..2	Cold trap	2	LH_2-cooled, 100mm i.d.
BS3..5	Cold trap	2	LH_2-cooled, 160mm i.d.
PT1..30	PMT-6-003	30	Thermocouple gauge, 1..10^{-3}Torr
PM1..28	PMM-46	28	Ion. gauge, 10^{-3}..10^{-9}Torr
PM35..37	PMM-32	3	Ion. gauge, 10^{-3} ..10^{-9}Torr
VE1,2	KVUM-16L	2	Air inlet
VH1..3	Dy-25 Gate valve	3	
VM1..4	2EVE-100 Gate valve	4	
VM10..26	VEP-63 Gate valve	17	
VM30..51	VEP-25 Gate valve	22	
VM60..65	NET	6	Controllable leak
VT1...8	750mm clearence valve	8	
VT10...12	630mm clearence valve	3	
VT20...27	ZPT-250 gate valve	8	Bakeable valve
VT30...40	ZPT-160 gate valve	13	Bakeable valve

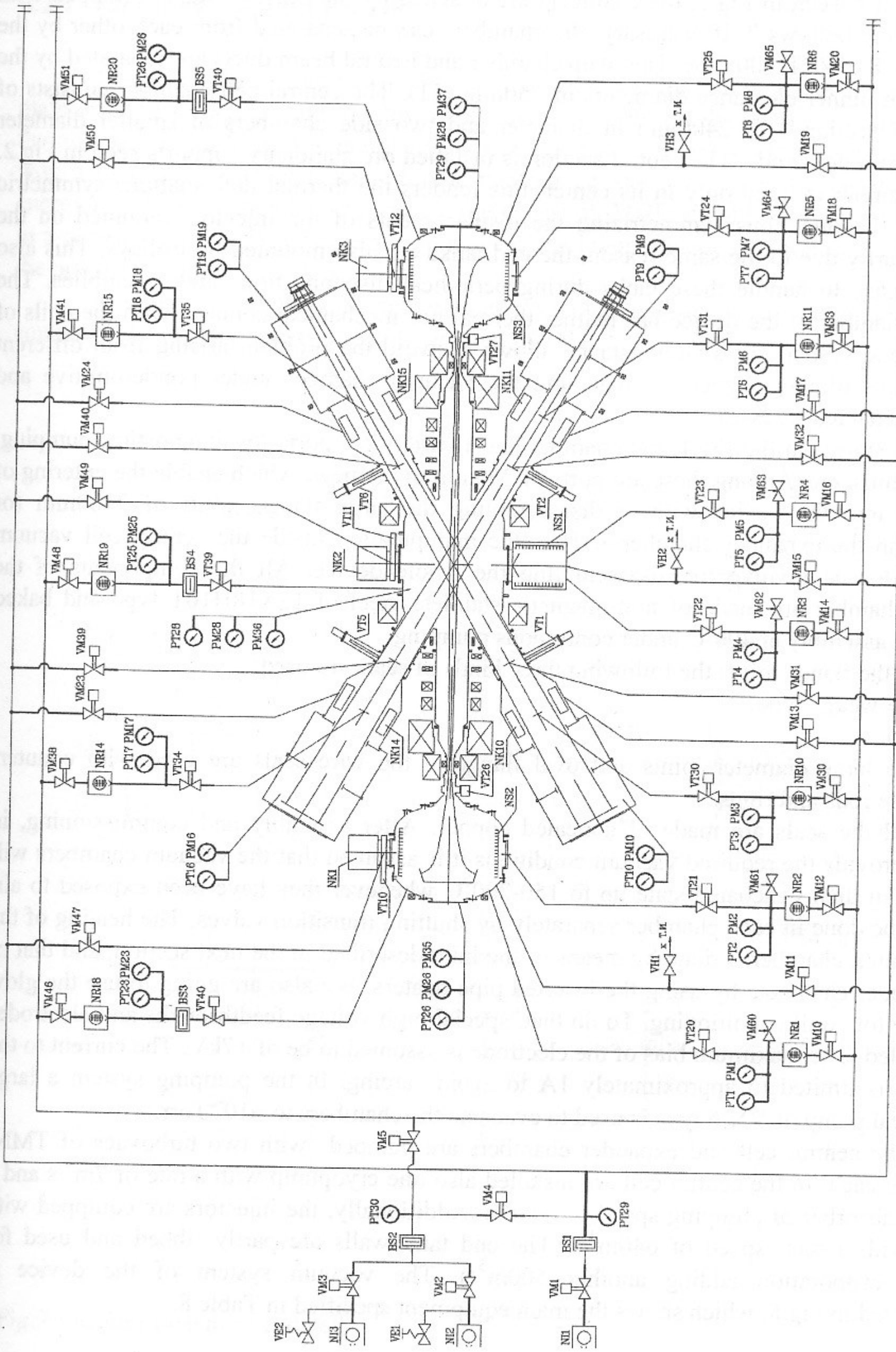

Fig.8 The HPNS vacuum system, specifications are given in Table 8.

As it is seen in Fig.1, the chambers are attached by the mirror units 2 equipped with compensating bellows 7. If necessary, the chambers can be separated from each other by the gate valves 8 of ZPT-200 type. The main chamber and neutral beam ducts are separated by the valves with innner clearance diameters of 750mm (11). The central cell chamber consists of the central section 3 of 2400mm in diameter and two side chambers of smaller diameter attached from both ends. The central section is installed on stationary supports seen in Fig.2. As the chamber is fixed only in its center, this renders the thermal deformations symmetric during the heating, thus symmetrizing the displacements of the injectors mounted on the trolleys. Partly due to the same reason, the end tanks are also mounted on trolleys. This also makes it easy to handle these tanks during periodical disconnections and assemblies. The vacuum chamber of the device has neither thermal nor mechanical contacts with the coils of the magnetic system. This circumstance allows to avoid the problem arising from different deformations of the magnetic system and the vacuum chamber under ponderomitive and thermomechanical stresses.

As shown in the Fig.1, the chamber has a variety of ports for diagnostics, pumping, neutral beams, etc. Among these are ports of 750mm in diameter which enable the entering of personnel into the device without disassembling the large flange joints of 2400mm (or 2600mm in the expander chambers). Thus the manipulation inside the central cell vacuum chamber doesn't involve for disassembling the whole device. All the components of the vacuum chamber are made of non-magnetic stainless steel of 12X18H10T type and baked before the assembly at 400°C under continuous pumping.

In the flange joints the following three kinds of seals are used:

1. Groove-wedge type;
2. CF-type;
3. For the large diameter joints and oval flanges - the wire seals are used with counter-sinkable rods and rings.

All the seals are made of annealed copper. After assembly and commissioning, in order to provide the required vacuum conditions it is assumed that the vacuum chambers will be baked in their evacuated state up to 150-200°C whenever they have been exposed to air. This can be done in each chamber separately by shutting transition valves. The heating of the main vacuum chamber is done by means of the liner described in the next section, and that of the expander chambers by using the inserted pipe-heaters. We also are going to use the glow discharge for wall conditioning. To do that, special high voltage feedthroughs and electrodes are installed. The maximum bias of the electrode is assumed to be of +7kV. The current to the electrode is limited to approximately 1A to avoid arcing. In the pumping system a large mechanical pump of VN-6 type is used to evacuate the chambers to $\approx 10^{-2}$Torr.

The central cell and expander chambers are pumped with two turbovacs of TMN-1500 type each. In the central cell are installed also one cryopump with a rate of $7m^3/s$ and a titanium absorber of pumping speed of $50m^3/s$. Additionally, the injectors are equipped with pumps with a total speed of $640m^3/s$. The end tank walls are partly ribbed and used for titanium evaporation adding another $500m^3/s$. The vacuum system of the device is schematized in Fig.8, which shows the main equipment specified in Table 8.

4.2.1 End tank vacuum system

It is necessary to pump away the gas released inside the end cell vacuum chamber. The main reason for rapidly pumping away the gas is to minimize the charge-exchange losses of the plasma leaking from the central cell. These occur since when a relatively fast ion collides with a molecule or atom it can become neutralized and substituted by an extremely low energy ion. This has an adverse consequence to overall MHD stability of the system. It results in a decrease of plasma pressure which reduces the favorable contribution of the expander to the pressure-weighted curvature.

A schematic of the end cell with the vacuum equipment is shown in Fig.9. The equipment components were already specified in Table 8.

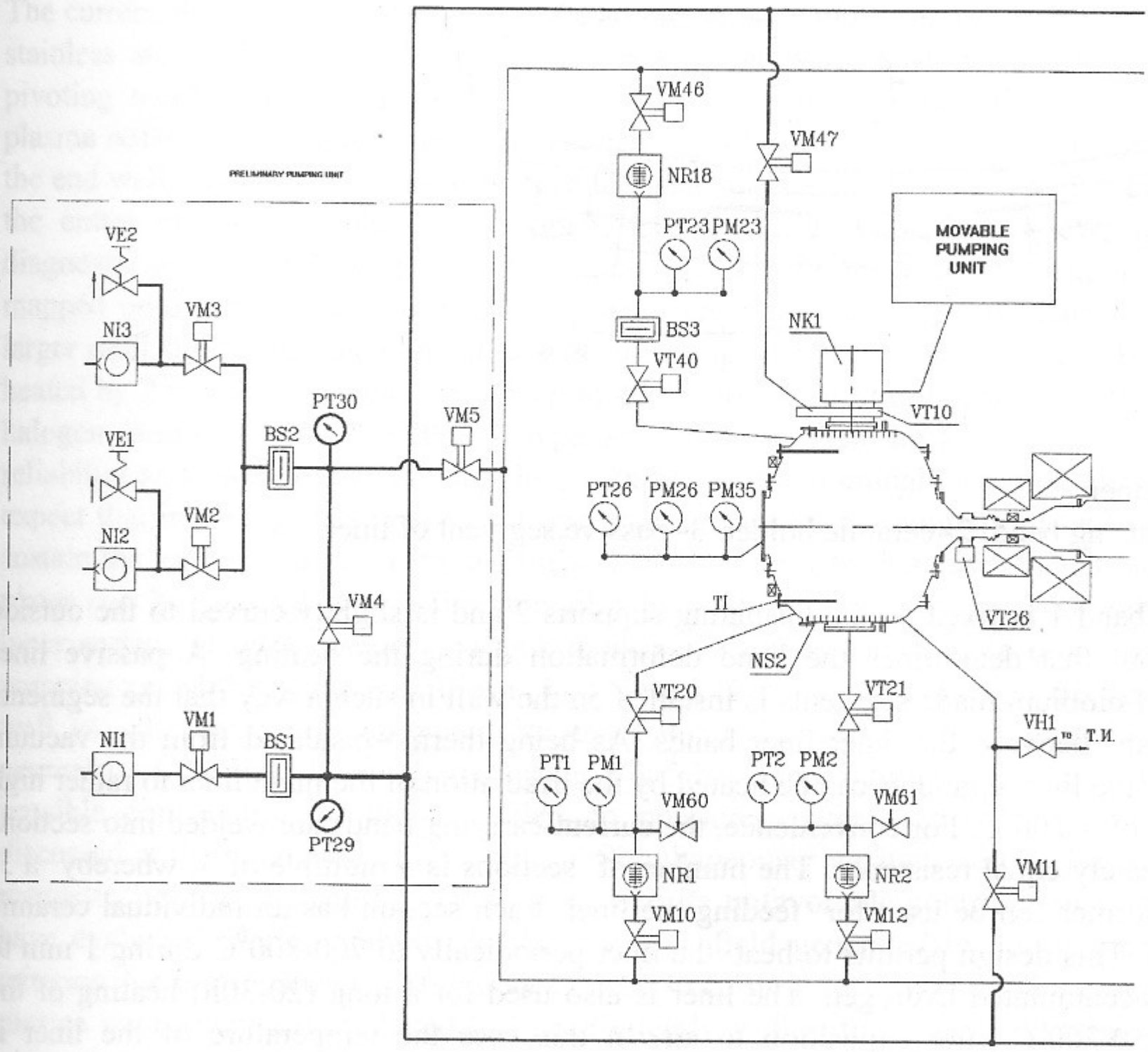

Fig.9 Vacuum system of end cell

4.2.2 First wall

In order to reduce the desorption of hydrogen from the chamber walls the central cell (about $45m^2$) is coated from the inside with a niobium liner. The liner is made of insulated plates and can be heated directly up to 800^0C by a current. It is expected also that the fast neutrals from the plasma impinging on the liner will be implanted and buried into the niobium. The liner of such a design was first made and tested electrically on the AMBAL device /28/. Structurally, the liner is made of niobium band of 0.3mm x 50mm (see Fig.10).

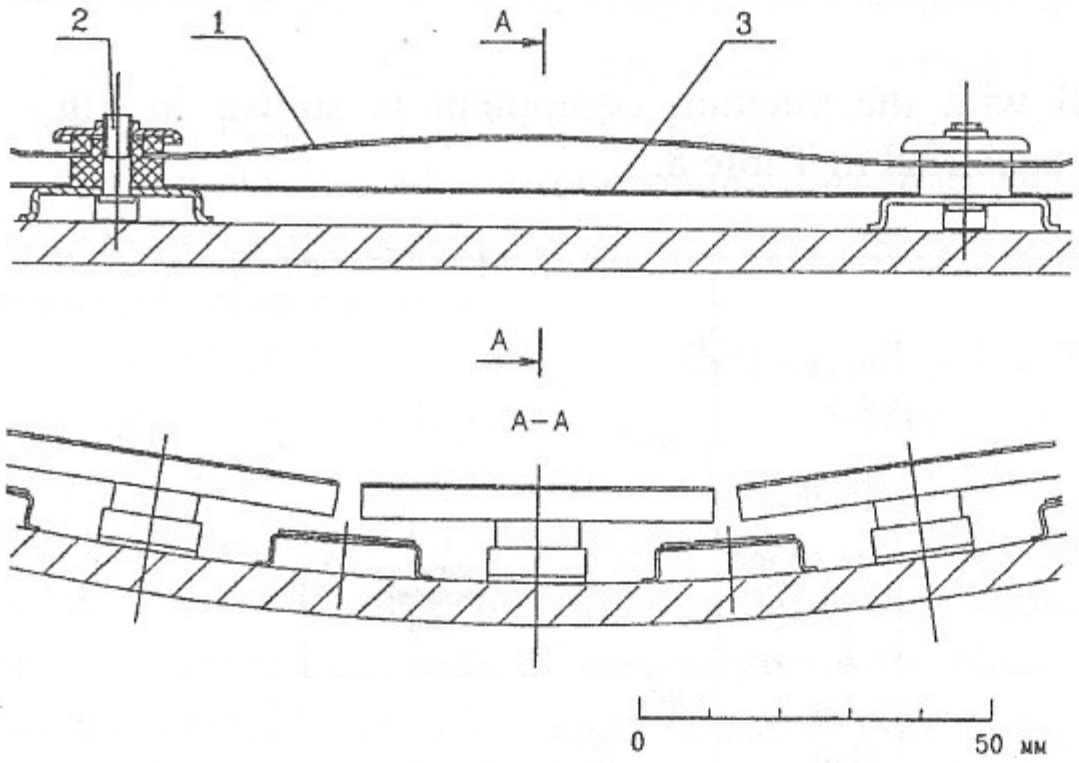

Fig.10 Nb-Liner
1- current-carring bend; 2- ceramic holder, 3- passive segment of liner

The band 1 is fixed on the insulating supports 2 and is slightly curved to the outside from the wall that determines the band deformation during the heating. A passive liner consisting of niobium made segments is installed on the wall in such a way that the segments cover the gaps between the outer liner bands. As being thermo-insulated from the vacuum wall the passive liner segments can be heated by the irradiation of the main liner to rather high temperature of $\approx 200^0C$. For convenience, the current-carrying bands are welded into sections of approximately equal resistance. The number of sections is a multiple of 3, whereby a 3-phase transformer can be used for feeding the liner. Each section has an individual ceramic feedthrough. This design permits to heat the liner periodically to $700\text{-}800^0C$ during 1 min to release the accumulated hydrogen. The liner is also used for a long (20-30h) heating of the vessel to $150\text{-}200^0C$ after exposition to air. In this case the temperature of the liner is approximately 400^0C.

4.2.3 End plate and limiter

The plasma leaking from the central cell through the mirrors is absorbed by the plasma dumps shown schematically on Fig.11. One of the conditions in its designing was that the surface of the dump is to be oriented approximately at 90^0 to the plasma stream in each point. The position of the dump was chosen according to different limitations imposed by plasma stability and longitudinal heat losses. The magnetic field at the end wall should be sufficiently small ($B/B_{max} < 1/40$) to provide a plasma expansion sufficient to supress electron heat

conductivity in the expander. On the other hand, the magnetic field near the wall can not be too small. Otherwise the ratio between the curvature radius and the ion Larmor radius is increased beyond that appropriate for the MHD approximation. This may introduce some ambiguity in predictions of the plasma stability. In certain cases the limitation on the maximum admissible ratio between the plasma radius and the Larmor radius of escaping ions becomes important. We have used the limitation on the curvature radius $\kappa\rho_i \leq 0.3$, where κ is a normal curvature introduced in the preceeding sections, that is consistent with the value measured in the GDT experiment /29/.

The plasma dump consists of four concentric outer annular plates and a segmented flat back plate, electrically insulated from each other. Each annular ring is also divided azimuthally into 8 insulated segments. All the segments can be biased at an appropriate voltage to control a plasma potential profile in the central cell or can be grounded or floating. The current flowing to each end plate can be measured separately. The end plates are made of stainless steel of 12X18H10T type. The plates can be rotated independently by using a pivoting mechanism shown on Fig.12,13. That is needed because the angle at which the plasma strikes the wall, as already mentioned, is to be close to 90° over the entire surface of the end wall. Each plate serves to receive the plasma escaping from different radial regions of the entire volume and therefore should be properly pivoted. This allows to meet both diagnostic and control needs. As it is seen from Fig.11 the plasma occupying the region mapped onto the midplane to radii less than 1cm hits a disk-shaped plate 9. Plasma from larger radii flows onto the conical part of the dump. If needed the plates can be periodically heated by 25 quartz halogen lamps 5 up to 400°C for degassing. For heating of the plates the halogen lamps of KG 220-2000-2 type are fixed on their back sides. To increase their reliability and lifetime they are supplied with half of the nominal power, totalling 25kW. We expect that in a long pulse regime of operation enhanced pumping speed will be required to sustain the gas pressure near the wall less than 10^{-3}Torr. For that case the surface of the end plates can be covered with a titanium film by using arc evaporators 6. Simultaneosly, the inner surface of the expander end tank is also covered by titanium. In order to increase the pumping speed this surface is ribbed (7). Shield 8 is envisaged to protect the quartz lamps as well as the electrical equipment located behind the end plates against Ti-vapour. The geometry of the field lines shown on the Fig.5 has been optimized to obtain the maximum possible contribution of the expanders to pressure-weighted curvature under restrictions discussed at the beginning of this section. Simultaneously we have adjusted the profile of the magnetic field in the central cell to minimize its unfavorable contribution to stability. We have evaluated plasma stability in the magnetic field generated by the magnets using the criterion for the localized MHD-modes /1-3/. According to these considerations, the HPNS plasma parameters are predicted to be sufficiently well within the stable region. A detailed view of the plates supporting structure is given below in Fig.12,13.

There are fixed and movable plasma limiters defining the outer plasma edge at several positions along the magnetic field. Those are made of stainless steel. The movable limiter is assumed to be located behind the mirror unit. Its possible design which is to be tested on GDT is shown in Fig.14. The limiter ring is divided azimuthally into 12 segments which are conventionally floated electrically and may be biased, if necessary. Movable blades (14) can be inserted radially using a remote handling system shown on Fig.14. It comprises servo motor 1 and the gearing mechanism which includes two perpendicular rotating torsion rods mounted on the bear supports.

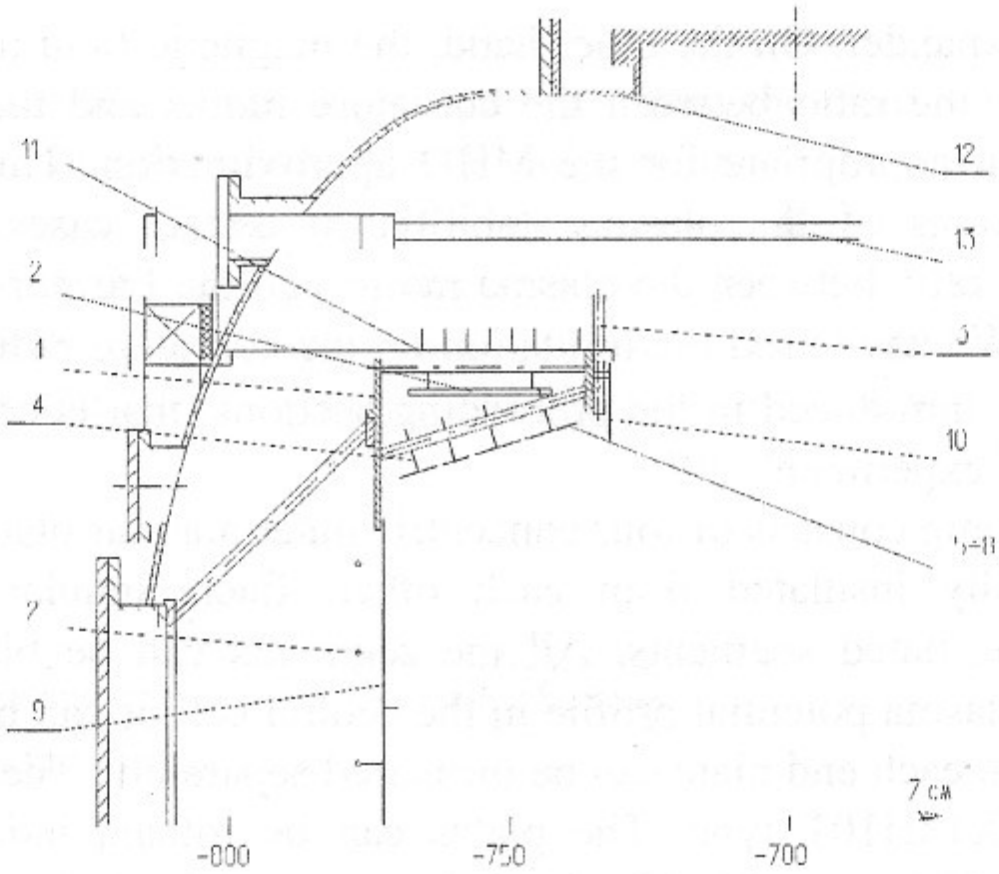

Fig.11 Plasma dump: 1 - mounting flange; 2 - quartz lamp; 3 - supports; 4 - pivoting unit; 5-8 - end plate segments; 9- back plate; 10,11- screens; 12- chamber wall; 13- Ti-evaporators

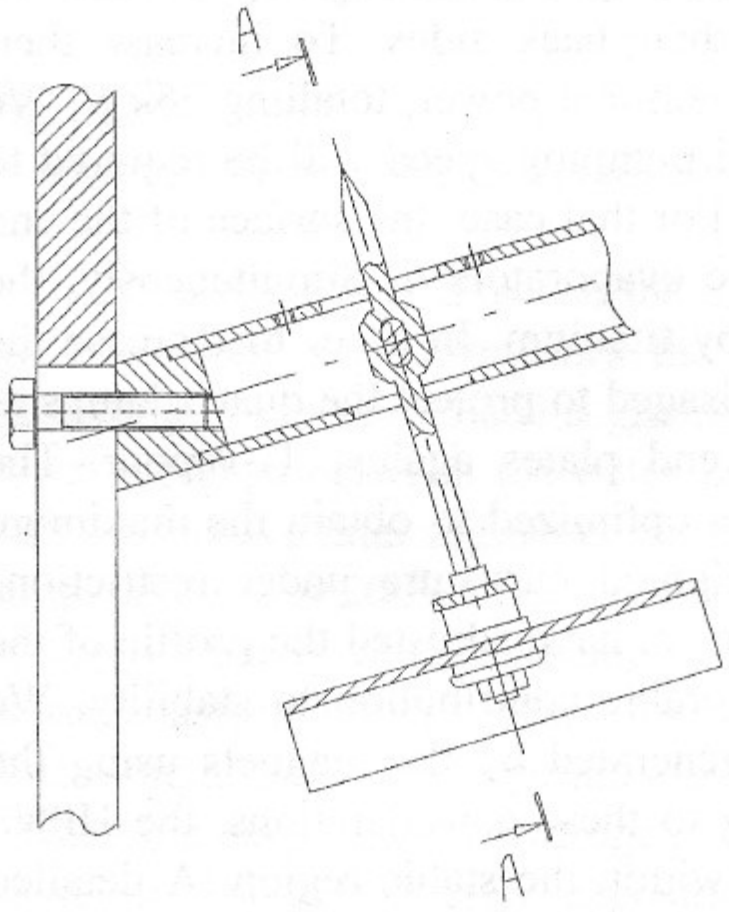

Fig.12 Pivoting mechanism of the end plates

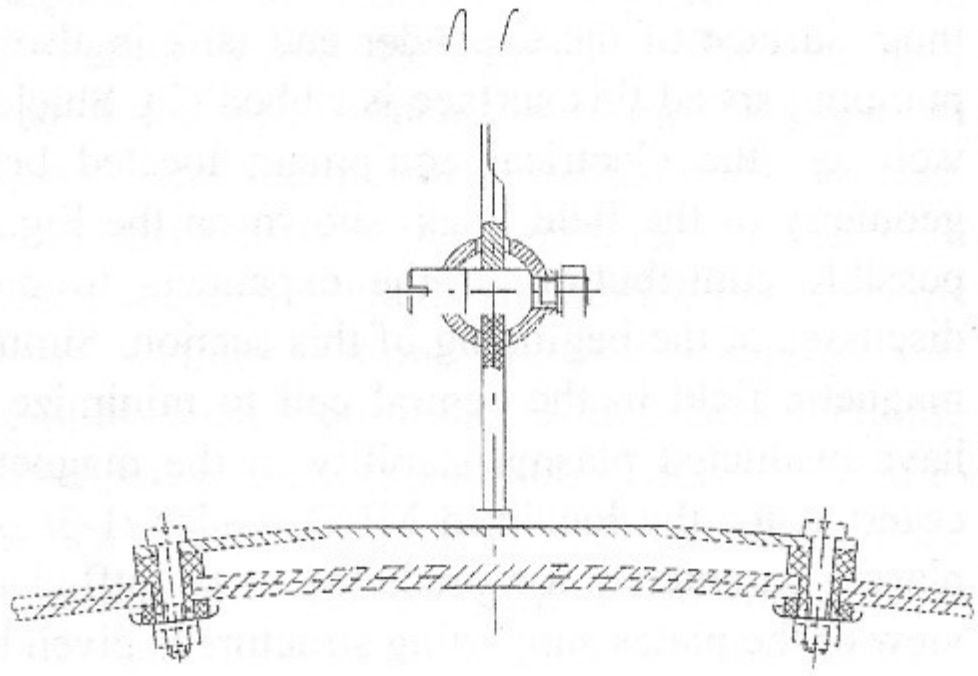

Fig.13 Evacuated view (90^0 rotated cut- away view of the pivoting end plate segment)

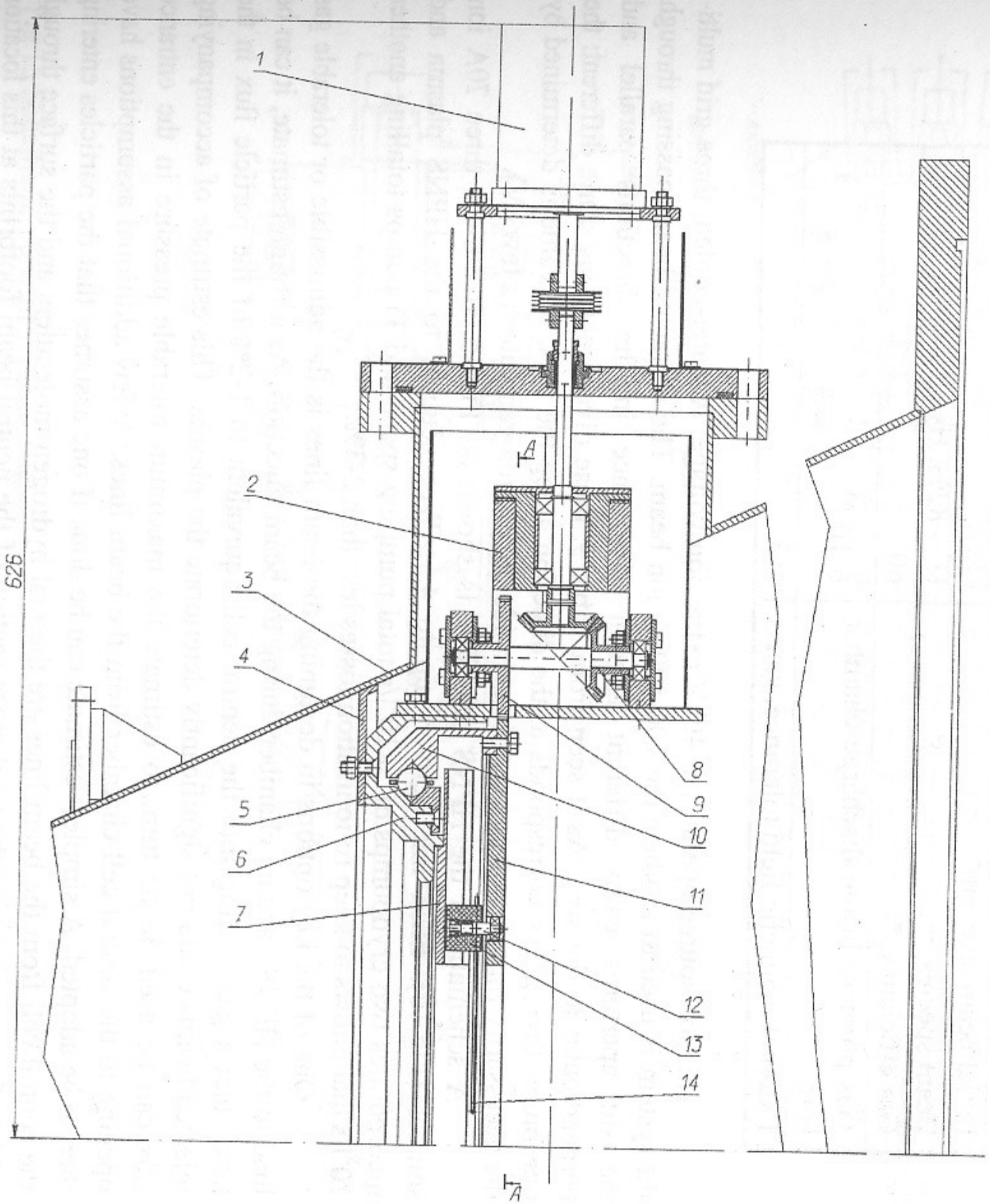

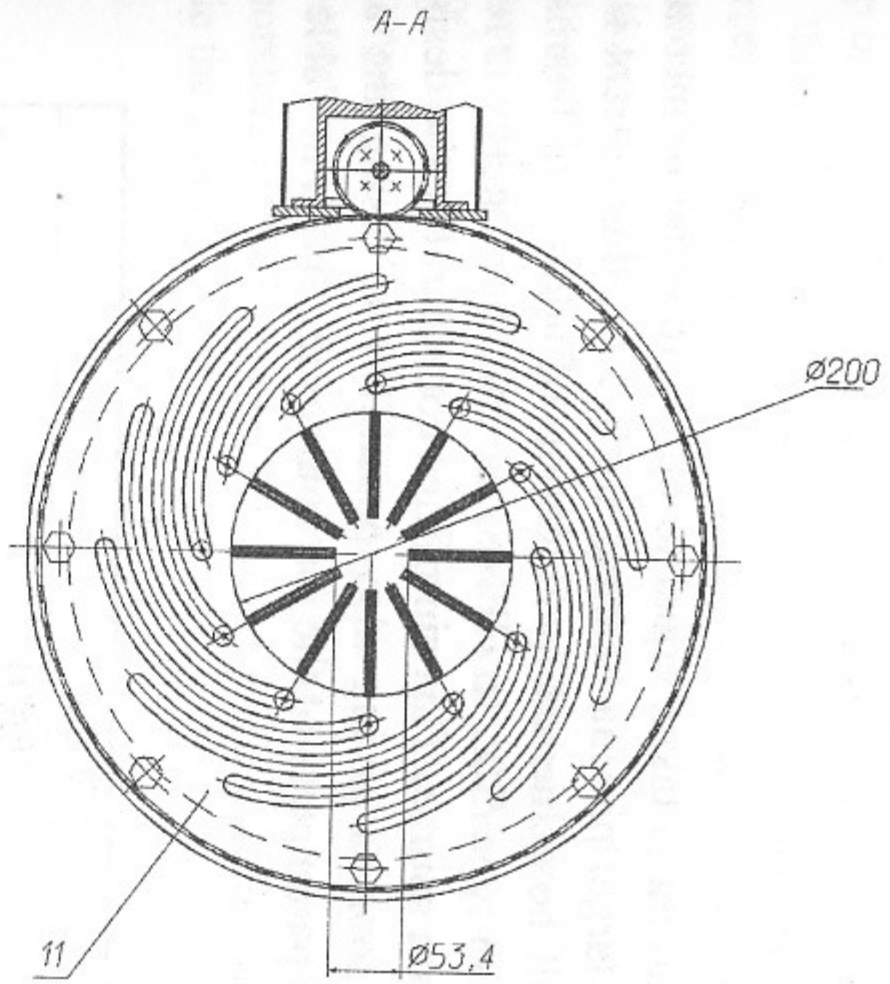

Fig.14 Movable Limiter

1. Servo motor DVSH80-06 2. Reducer
3. Vacuum chamber 4. Disk 5. Spherule
7. Disk with radial slots 8. Cone gear 9. Gearing
10. Support 11. Rack wheel 12. Axis of rotation
13. Slide 14. Limiter segment

4.3 Neutral beam system

The total equivalent injection current is taken equal to 600A. In order to increase the electron temperature in initial phase of target plasma heating, for 1-5ms, this current is to be increased by a factor of 1.5-2. This will be achieved by injection of additional beams from pulsed injectors, presumably of START-3 type /30/. In HPNS, the injection energy is reduced to 30-40keV in comparison to the neutron source. This simplifies considerably the design and the power supply system of the ion sources giving also possibility of using the already available sources of IPM-type /31/. The parameters of the ion sources are listed in Table 9.

Table 9 Ion source parameters

Parameter	Value
Extracting voltage, kV	30(40)
Ion current, A	70
Beam divergence, deg.	±2,±0.5
Pulse duration, s	up to 0.1
Extraction area, cm^2	144
Initial beam size, cm^2	12x25
Beam species	H^+ - 82%, H_2^+ -15%, H_3^+ -3%
Gas efficiency, %	60
Gas pressure inside discharge chamber, Torr	$6 \cdot 10^{-3}$
External magnetic field tolerance, gauss	1-3

This ion source operates at 40kV extraction voltage. A water-cooled, three grid multi-slit system is used to produce the 100-500ms ion beam. The extracted beam passing through the slit apertures gains different angular divergence in the directions parallel and perpendicular to the slits. As it seen from Table 9, these divergences are quite different: the minimum divergence corresponds to the direction along the slits. Its value is determined by the necessarily finite temperature of ions inside the plasma generator (a few eV).

A schematic of the HPNS beamline is shown on Fig.15. It utilises three 70A ion sources (Fig.16). Each line delivers up to 4.5MWof neutrals to the HPNS plasma and incorporates two cryopumps of 5×10^5l/s total pumping speed and Ti-pumps totalling another 10^5l/s that allows to keep re-ionization losses less than 2-3%.

One of the key options in designing the beam lines is the admissible or tolerable gas load to the HPNS vacuum chamber during the beam injection. As a rough estimate, it can be taken that a gas puffing into the central cell equivalent to 1-2% of the particle flux in the injected beams could not significantly deteriorate the plasma. This estimate of accompanying flux can be used, in its turn, to estimate the maximum tolerable pressure in the entrance opening to the central cell chamber from the beam lines. A few additional assumptions have then to be adopted. A simplest estimate can be done if one assumes that the particles entering the central cell from the beam lines are thermal hydrogen moleculers and the surface through which they pass is twice the total cross-section of the neutral beam footprints at this location (accounting the beam divergence it is roughly equal to 10^3 cm^2). Such a consideration gives the maximal tolerable pressure of 3×10^{-6}-10^{-5} Torr. In order to provide the required pressure

drop of the gas flowing out from the ion sources and neutralizers differential pumping is used. For this purpose the vacuum chamber is divided into 5 sections. Section 1 contains ion sources and neutralizers placed immediately downstream of the extraction system. Section 2 houses bending magnets and others house the beam funnels. The pressure in Section 1 during the beam pulse should not exceed 10^{-4}Torr. If it will be higher some adverse consequences might occur to extraction grids. The unneutralized ion beams emerging from neutralizers enter Section 2 where they are deposited on the beam dumps. In Sec. 2 and 3 the pressure will be $5x10^{-5}$ Torr , reducing to 10^{-6} Torr in the downstream sections 4,5. The gas in the injector tank is pumped out by two helium cryopumps with with pumping speed of 3×10^5 l/s and 2×10^5 l/s in sections 1 and 2 respectively, and by water-cooled panels coated by Ti using arc evaporators ($100m^2$). The Ti-coated panels additionally provides 1×10^5 l/s of pumping speed inside the second section.

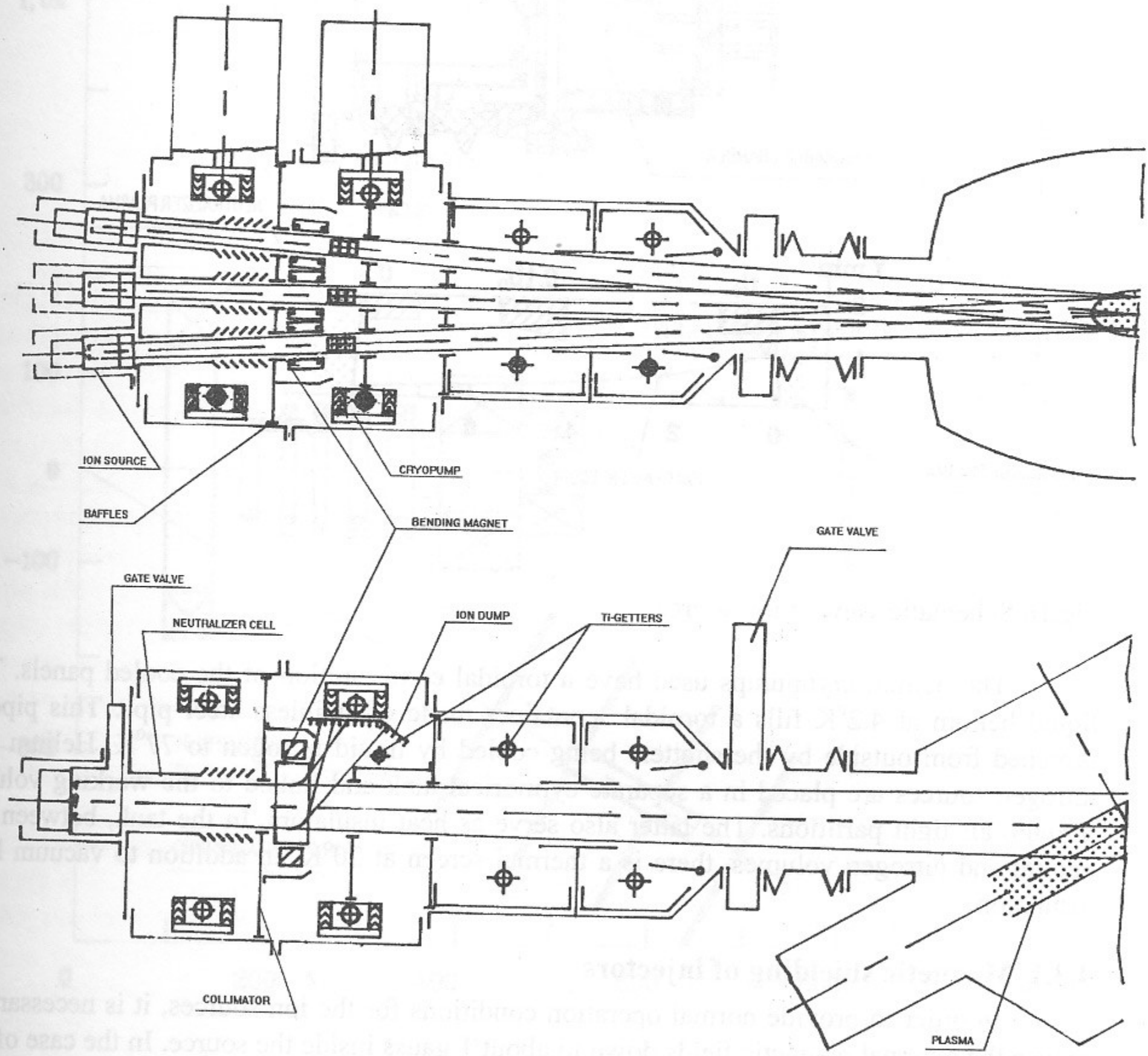

Fig.15 Schematic view of injector tank

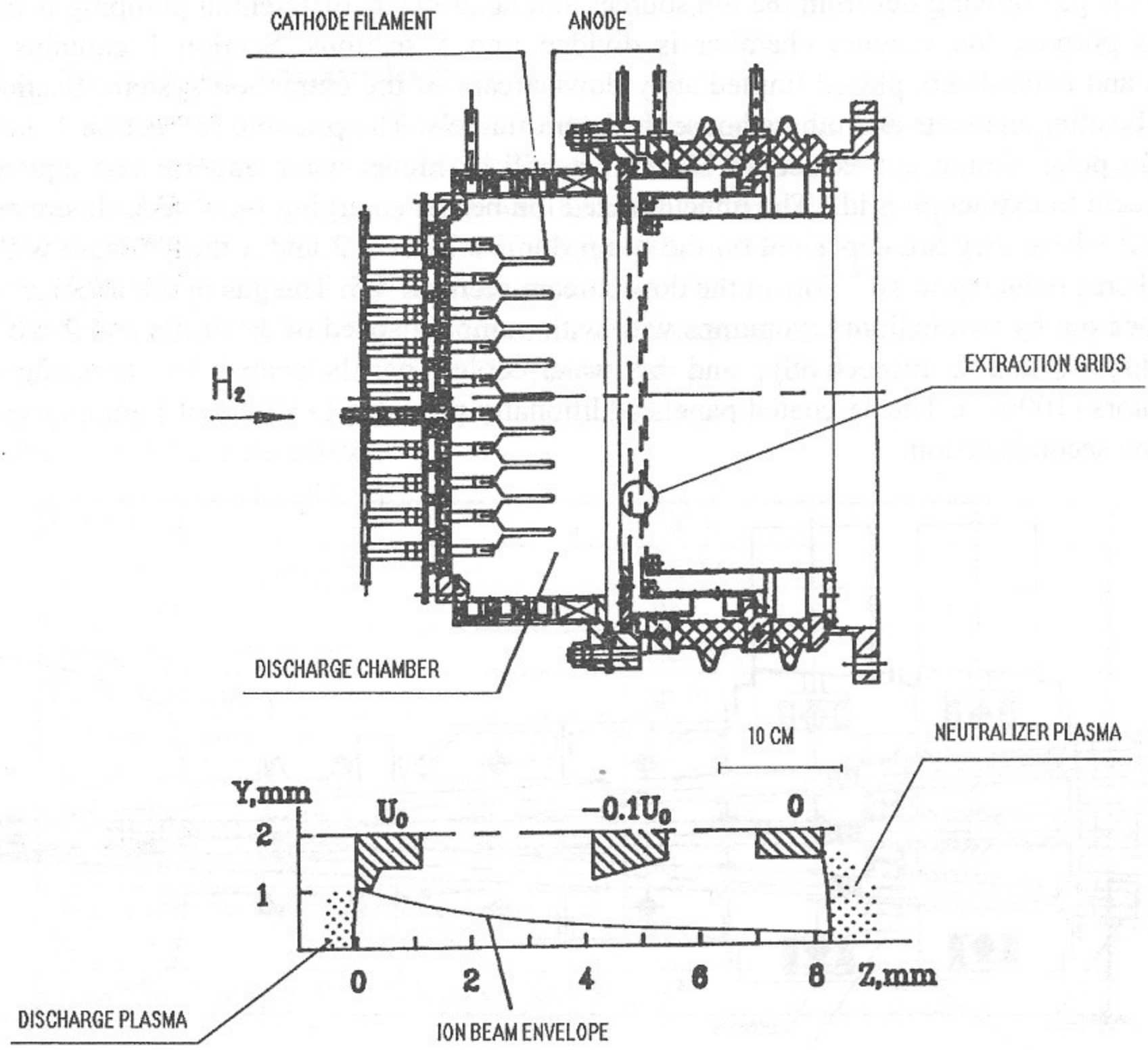

Fig.16 Schematic view of ion source

The helium cryopumps used have a toroidal configuration of the cooled panels. The liquid helium at 4.2°K fills a toroidal container made of stainless steel pipe. This pipe is screened from outside by the shutters being cooled by liquid nitrogen to 77°K. Helium and nitrogen sources are placed in a separate cylindrical tank and linked to the working volume through air tight partitions. The latter also serve as heat insulators. In the tank, between the helium and nitrogen volumes, there is a thermal screen at 20°K, in addition to vacuum heat insulation.

4.3.1 Magnetic shielding of injectors

In order to provide normal operation conditions for the ion sources, it is necessary to reduce the external magnetic fields down to about 1 gauss inside the source. In the case of the Hydrogen Prototype, several factors turn the screening of the stray magnetic field into a rather complicated problem. These factors are:

1. the magnetic system of the HP device has a large magnetic moment unlike tokamaks;
2. the injection angle is 30°, i.e. the ion source is positioned close to the magnetic coils of one of the mirror units;
3. the mirror field is quite large approaching 20T on axis

These factors cause the necessity to screen the beam duct against 0.03-0.06T fields which have parallel as well as perpendicular components. If not screened, the transverse component of the external field in the separator is of the magnitude comparable with its own field in the gap. Obviously it can cause considerable distortion of the ion trajectories inside the separator. In the ion source region, the external field appears to be less ($H_{\parallel}$= 0.02T, $H_{\perp}$ =0.016T), nevertheless exceeding the value allowed for normal operation of the source. Such a large magnitude of the stray field dictates the application of two combined screening methods. Firstly, the local magnetic field is reduced by using a system of screening coils (see Fig.17) to a value which permits the use of ferromagnetic shields; secondly, residual fields are to be suppressed by the ferromagnetic screens inserted one into another. The calculated magnetic fields on the injector axis are also given here in Fig.18.

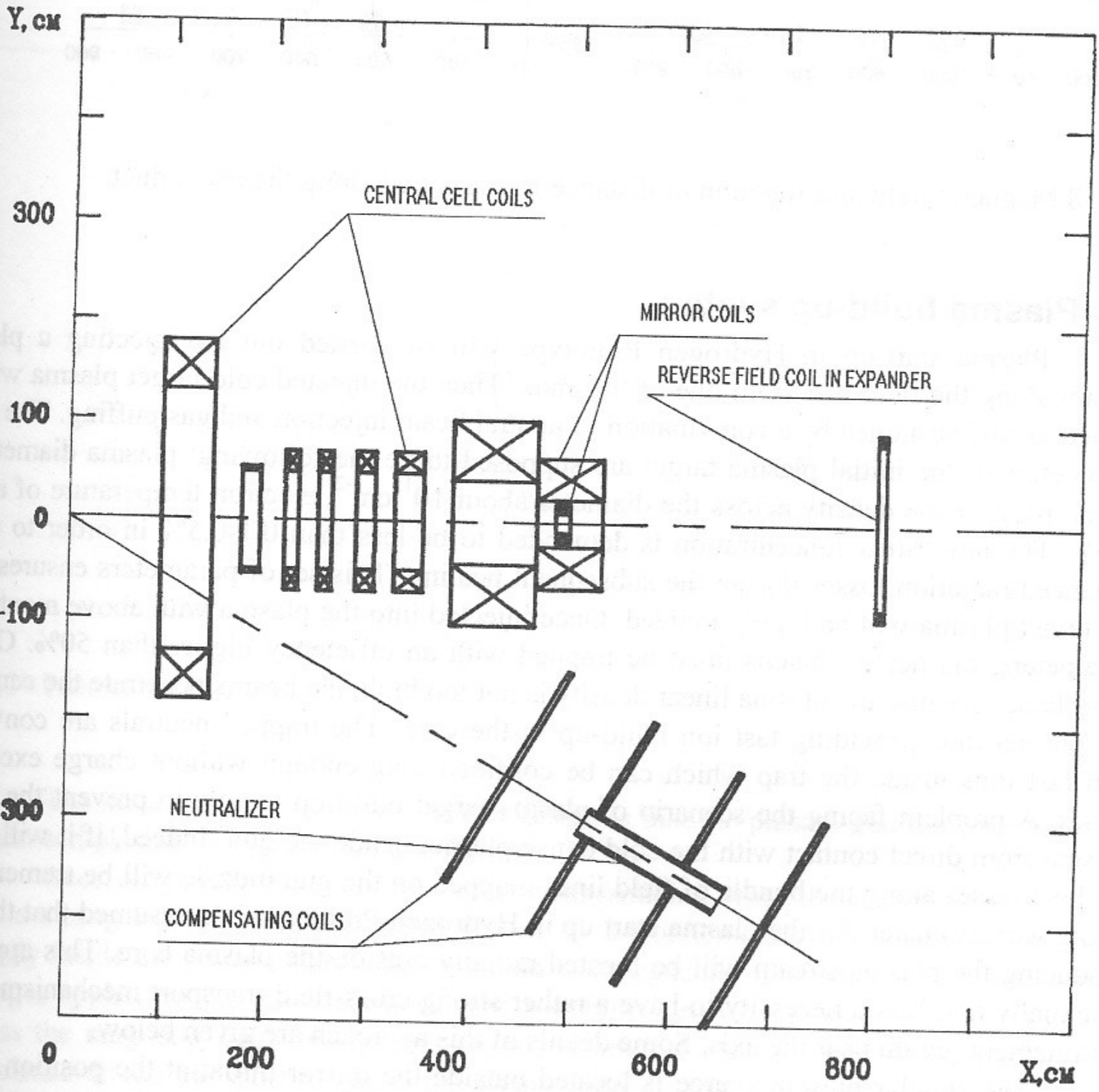

Fig.17 Locations of compensating coils

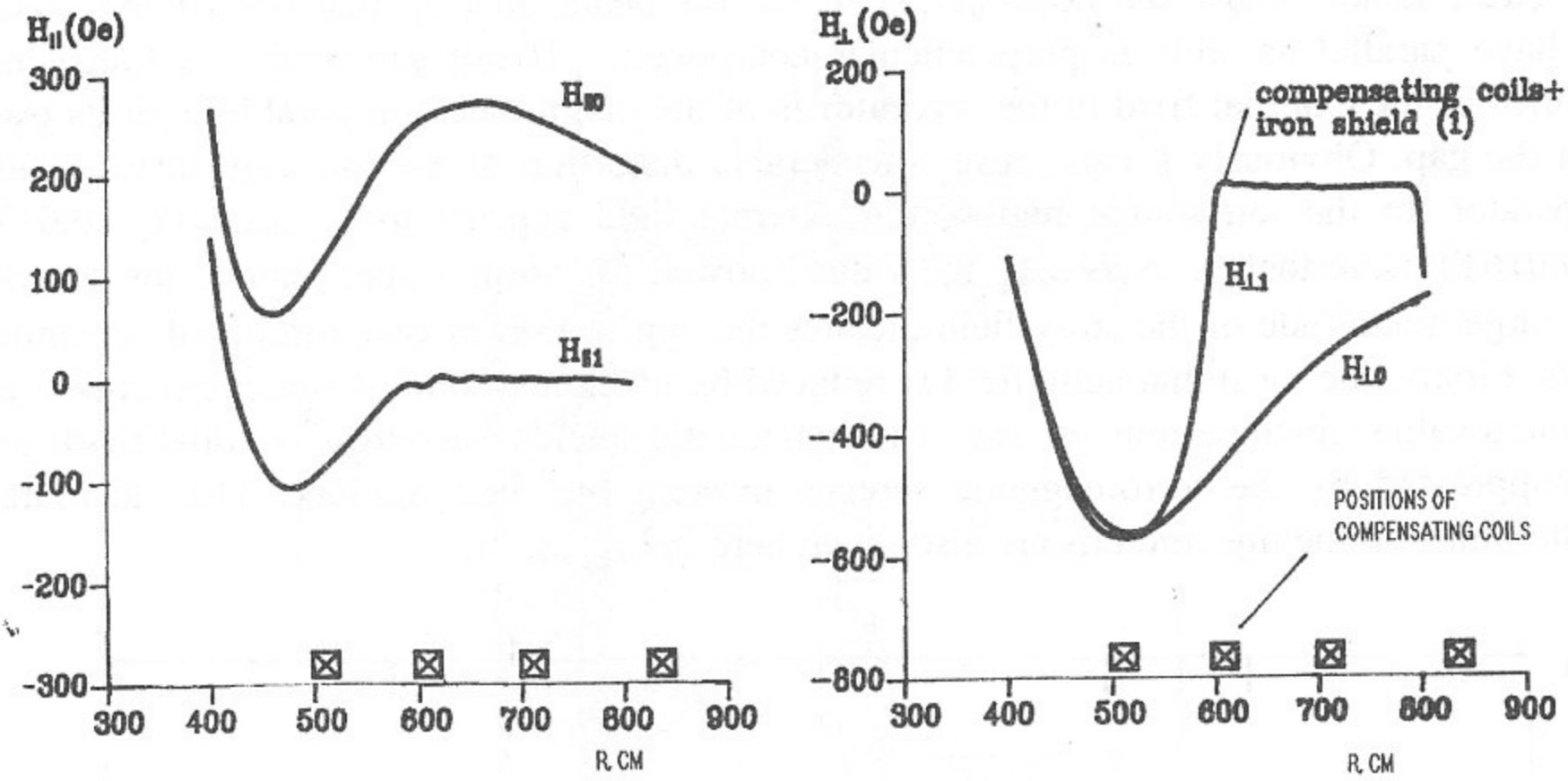

Fig.18 Magnetic field as a function of distance R, measured along the beam duct.

4.4 Plasma build-up system

Plasma start-up in Hydrogen Prototype will be carried out by injecting a plasma stream along the field line from one of the ends. Then the injected cold target plasma will be heated up and sustained by a combination of neutral beam injection and gas puffing. The main parameters of the initial plasma target are supposed to be the following: plasma diameter of 20cm, plasma line density across the diameter about $10^{15}cm^{-2}$, electron temperature of above 10eV. The impurities concentration is demanded to be less than 0.1-0.5% in order to avoid enhanced radiation losses during the subsequent heating. This set of parameters ensures that the target plasma will be highly ionized. Once injected into the plasma with above mentioned parameters, the neutral beams must be trapped with an efficiency higher than 50%. On the other hand, because the plasma linear density is not too high, the beams penetrate the center of the plasma thus providing fast ion build-up in the core. The trapped neutrals are converted into fast ions inside the trap which can be confined long enough without charge exchange losses. A problem facing the scenario of plasma target build up is how to prevent the target plasma from direct contact with the cold dense plasma inside the gun. Indeed, if it will occur the heat losses along the bundle of field lines mapped on the gun muzzle will be tremendous. In the scenario taken for the plasma start up in Hydrogen Prototype it is assumed that the gun producing the plasma stream will be located radially outside the plasma core. This approach essentially involves a necessity to have a rather strong cross-field transport mechanism to fill confinement region near the axis. Some details of this approach are given below.

The annular plasma source is located outside the mirror throat at the position where the magnetic field is $\approx$ 0.3 of the mirror field. The scheme of the plasma build-up system is shown on Fig.19.

The plasma source provides an annular plasma stream with ion current of a few kiloamperes and relatively small ion temperature. The initial radius of the plasma stream is fixed by the diameter of the gun muzzle and equials to 10cm whereas its radial extent is initially of the order of 1cm. Since the local mirror ratio is not too high, the magnetized plasma is transported through the mirror without significant reflection.

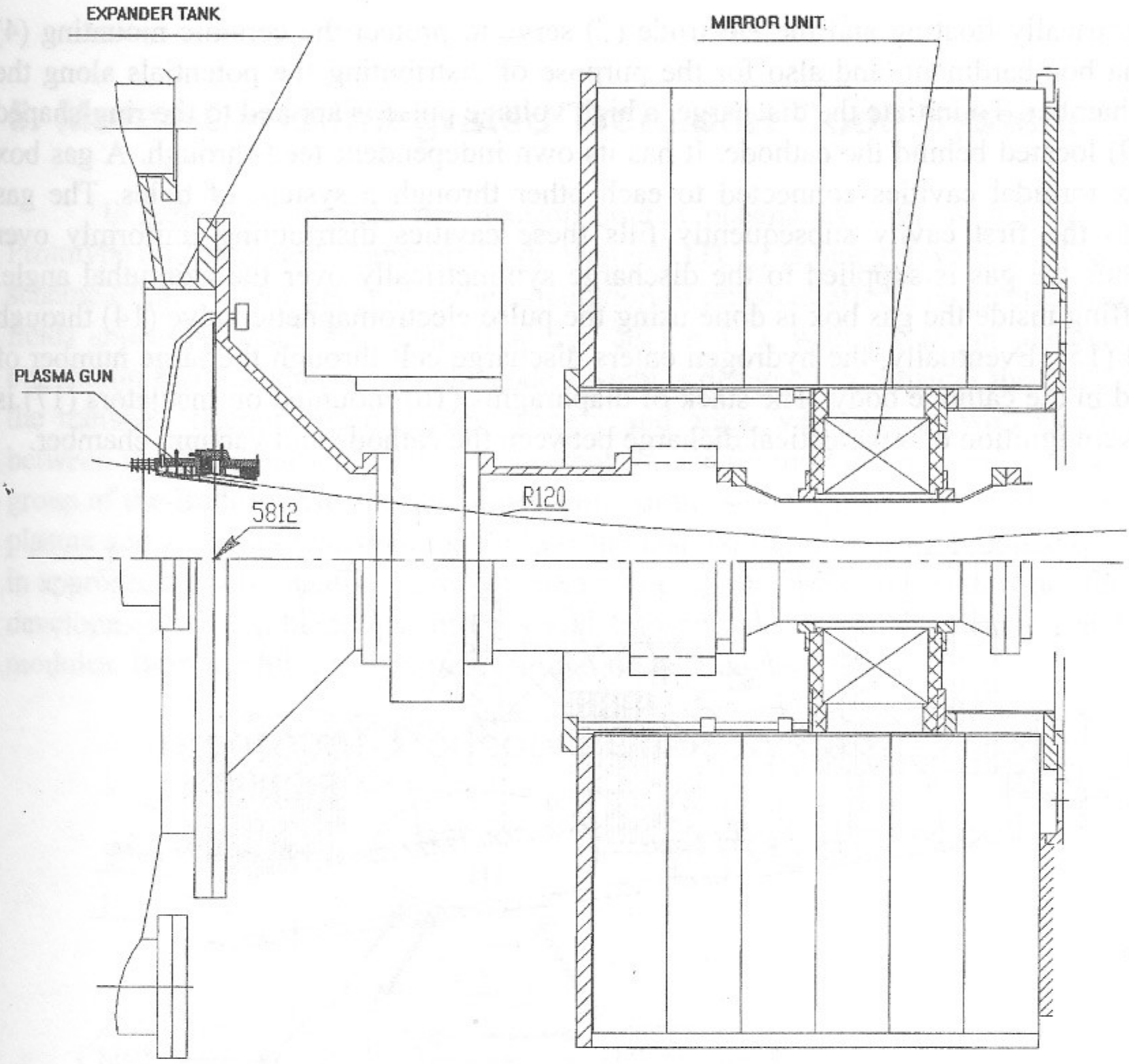

Fig.19 Plasma build-up system

The most remarkable feature of this design is that the plasma gun does not cut off the central cell plasma escaping into the expander.

According to the results of preliminary experiments, when the stream enters the central cell, a strong instability is developed driven by a nonhomogenious electric field directed radially inside the plasma slab /32/. This field is intrinsically imposed across the slab by the voltages applied to the gun electrodes. The instability growth causes rapid plasma transport across the magnetic field through the chaotic azimuthal electric field of fluctuations. This turbulence-driven transport results in the plasma build-up in the near-axis region of the central cell.

The plasma gun (see Fig.20) has a coaxial configuration with an annular anode and a cone-shaped cathode whose surfaces are adjusted be parallel to the field lines nearby. The inner cone which serves as a cathode is combined from the main part made of stainless steel (2). and a molymdenum ring-shaped insert (1). The outer cone comprises a few parts: massive molymdenum anode with removable insert (3); two stacks of molymdenum washers insulated from each other by ceramic spacers (6) and a conic electrode (7) made of stainless steel. The

washers electrically floating and the electrode (7) serve to protect the ceramic mounting (4) from plasma bombardment, and also for the purpose of distributing the potentials along the discharge chamber. To initiate the discharge, a high voltage pulse is applied to the ring-shaped electrode (9) located behind the cathode. It has its own independent feed-through. A gas box (12) has six toroidal cavities connected to each other through a system of holes. The gas injected into the first cavity subsequently fills these cavities distributing uniformly over azimuth. Thus the gas is supplied to the discharge symmetrically over the azimuthal angle. The gas puffing inside the gas box is done using the pulse electromagnetic valve (14) through the channel (15). Eventually, the hydrogen enters discharge cell through the large number of holes drilled in the cathode body. The stack of diaphragms (16) mounted on insulators (17) is used to prevent ignition of a parasitical dicharge between the cathode and vacuum chamber.

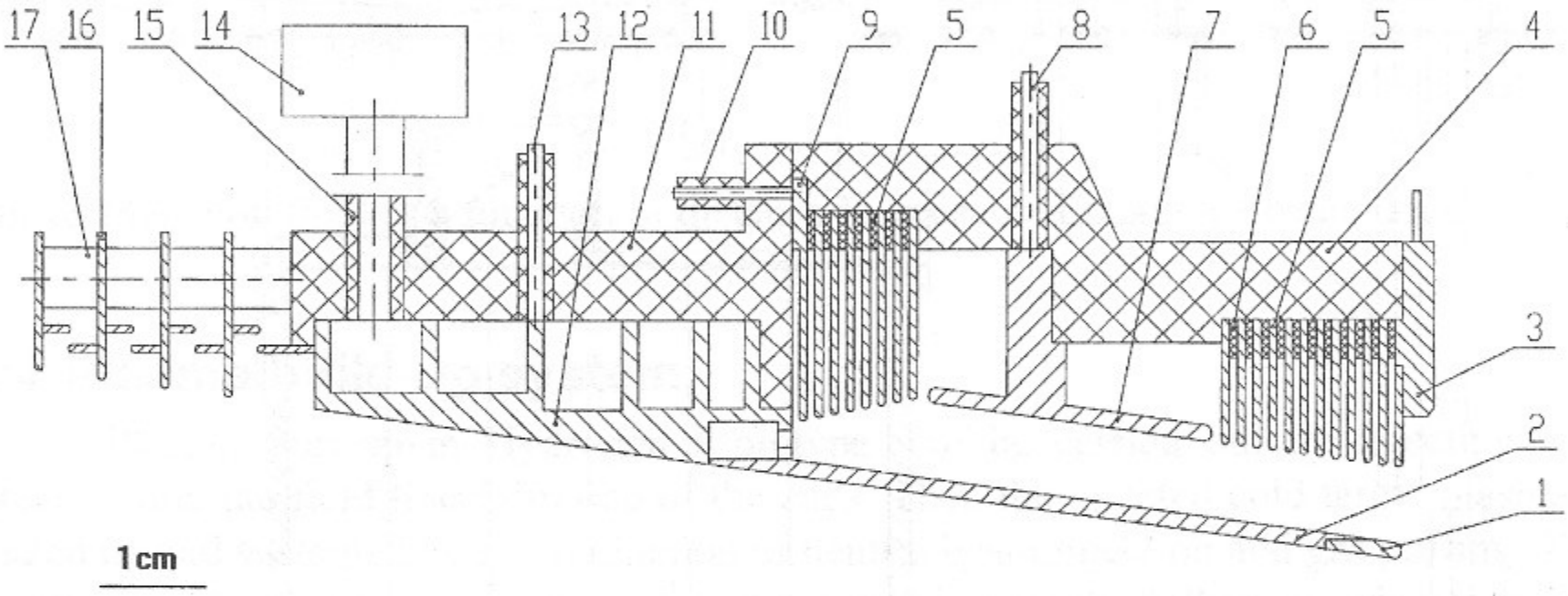

Fig.20 Plasma gun:
1 - cathode insert; 2 - cathode body; 3 - anode insert; 4 - insulator; 5 - molybdenum washers; 6 - ceramic spacers; 7 - floating electrode; 8,10 - electrical feed-through; 9 - electrode; 12- gas box; 13 - feed-through; 14 - pulse valve.

5. Monte-Carlo Integrated Transport Code System

In order to simulate the neutron source plasma as well as that in the Hydrogen Prototype an Integrated Transport Code System (ITCS) is being developed. Fig.21 shows the scheme of the system. Its goal is the calculation of physical effects connected with the particle fields appearing inside the neutron source device, i. e. with the target plasma, the fast ion population and the neutral gas. The code system is designed to consider the full dependence of the transport phenomena on space, energy and angle variables as well as the interactions between the three particle fields. At present the single modules are under development. The group of the Budker Institute elaborates a one-dimensional (in space) MHD code for the target plasma and a two-dimensional method for the fast ion module being founded on an expansion in appropriate, non-negative basic functions. The efforts in FZ Rossendorf are focussed on the development of mathematical models and transport codes for the fast ion and neutral gas modules. Both modules use particle simulation techniques /33/.

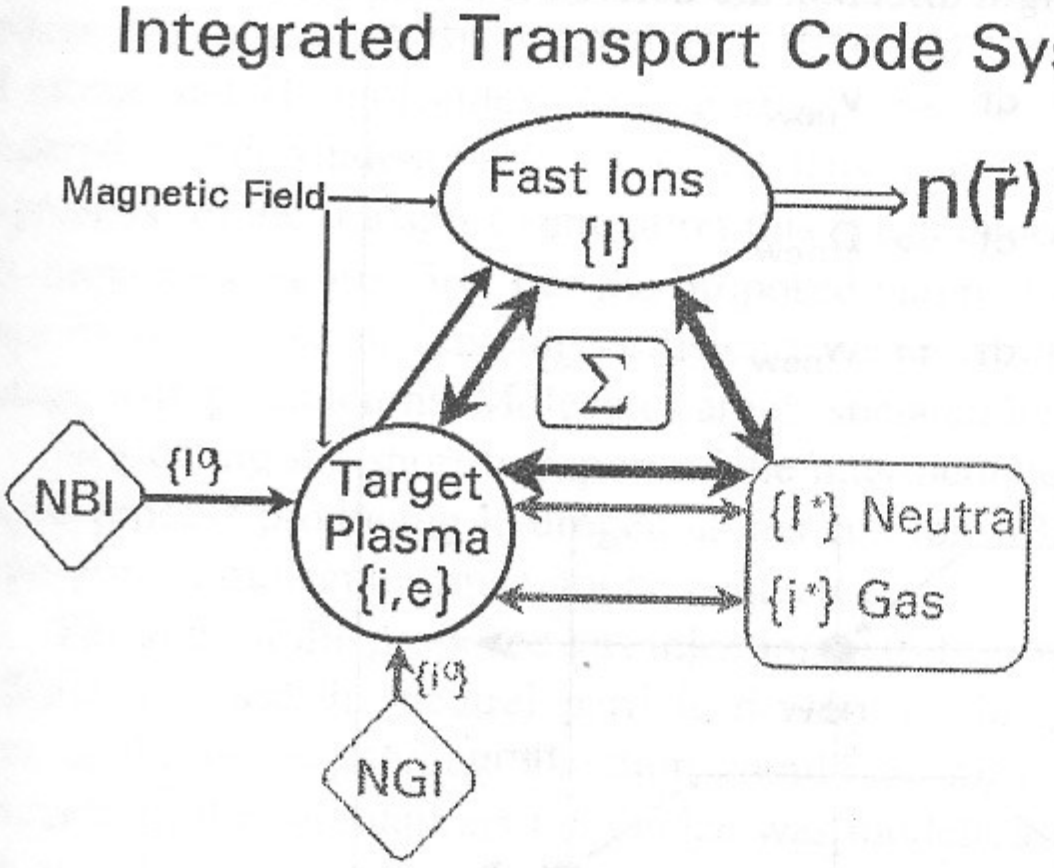

Fig.21 Scheme of the ITCS

Within the ITCS the fast ion module holds the central part because the field {I} of the fast ions ($I=D^+$, T^+ of 80-100 keV initial energy) determines the neutron source distribution $n(\vec{r})$. A first version of a Fast Ion Transport code (FIT) has been developed. It is based on the so-called background approximation assuming the (r, z)-profiles of densities and temperatures for both the target plasma and the neutral gas to be known and the direction dependences of these fields to be isotropic. The fast ion distribution function $f_i(\vec{r}, v, \vec{\Omega}, t)$ is then the solution of the Landau-Fokker-Planck equation 5.1:

$$\frac{\partial}{\partial t} f_I + \left[v\vec{\Omega}\frac{\partial}{\partial \vec{r}} + \frac{e}{m}\left(v\vec{\Omega} \times \vec{B}\right) \frac{\partial}{\partial \vec{v}} \right] f_I = \frac{1}{\tau_s * v^2} * \frac{\partial}{\partial v}\left(v^3 + v_c^3\right) f_I +$$

$$D_{II} * \left[\frac{\partial}{\partial \zeta}\left(1 - \zeta^2\right) \frac{\partial}{\partial \zeta} + \frac{1}{\left(1-\zeta^2\right)} * \frac{\partial^2}{\partial \varphi^2} \right] f_I - \langle \sigma v \rangle_{cx} f_I + S. \qquad 5.1$$

The streaming term on the left-hand side describes the motion of the ions under the Lorentz-force in an external magnetic field $\vec{B}$. The first and second term on the right-hand side model the moderation of the velocity v by the target plasma and the diffusion of the flight direction $\vec{\Omega}$ by ion-ion collisions, respectively. The latter contains a nonlinearity caused by collisions between fast ions. The third term represents their loss rate by charge-exchange processes with neutral gas atoms. S is the source distribution of the fast ions which is generated by the Neutral Beam Injection (NBI) into the target plasma. The parameters ($\tau_s, v_c, D_{||}$, and $\langle\sigma\ v\rangle_{cx}$) are calculated from the information about the target plasma and the neutral gas. The transport code FIT simulates stochastically independent fast ion histories in such a way that the mean of their distribution in phase space is just given by fI from Eq.1. For this end the simulation procedures of the diverse processes must be constructed in a well defined manner. The evolution of a history in time is simulated according to the leap-frog method illustrated in Fig. 22. Particle location and kinematic parameters v, with the statistical weight w are alternately calculated at times shifted against each other by half a time-step dt/2. The time-step dt is restricted by the stability criteria for the ion motion in the magnetic field. For this procedure the BORIS-algorithm /34/ is used. The coefficients determining the changes of the velocity and of the flight direction are derived from Eq.5.1.

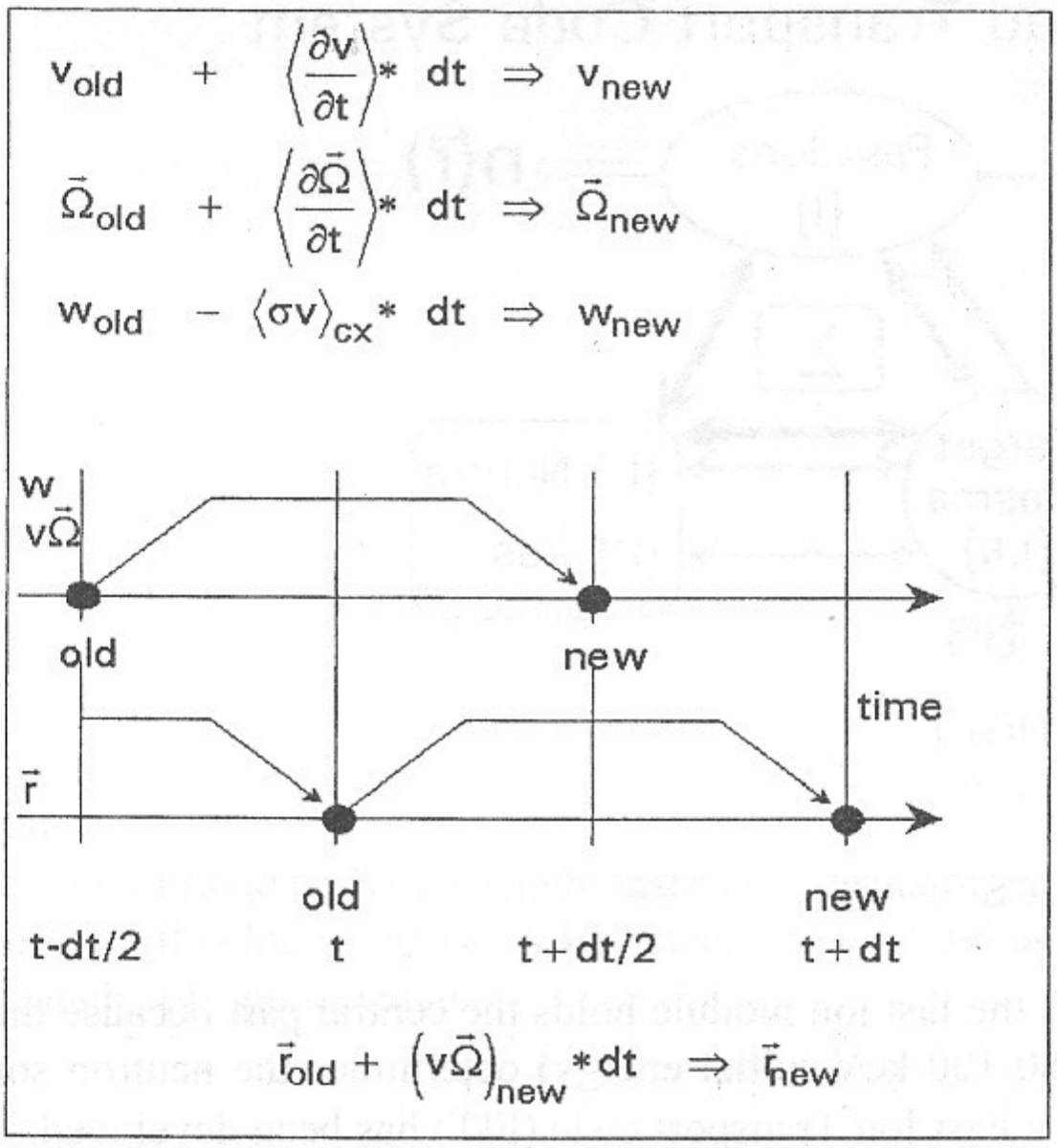

Fig.22 Particle transport simulation according to the leap-frog method

The code FIT is written in FORTRAN 77 with the special demand to maximally utilize the vector capability of the CONVEX C-3820 computer. It has been tested in a series of simplified model calculations. For the next step of the code development it is planned to introduce the time-dependence in the fast ion transport as well as in the target plasma and neutral gas description. This feature will allow to validate the mathematical models by comparing with results measured in experiments at the GDT facility.

5.1 Neutral gas simulation

The neutral gas contained in the central cell of the mirror device causes losses of fast ions as well as of plasma ions by charge-exchange processes. This is why the neutral gas transport is included in the ITCS. Notwithstanding this general goal of a neutral gas module the first phase of the code development was directed to the solution of an actual problem in the Hydrogen Prototype design. The target plasma continuously streams out of the central cell into the expanders (see Fig.1). For maintaining steady state conditions plasma has to be supplied. A possible method is the gas feeding. That means hydrogen gas is injected into and ionized by the plasma itself. Obviously, this method may be used only provided the plasma density is not too low. With the help of the developed code TUBE various versions of such a gas feeding device have been studied. TUBE simulates the linear neutral gas transport according to the Monte-Carlo method. The interactions with plasma and metallic walls are similarly treated as in the EIRENE code that has been developed for solving neutral gas problems in tokamaks /35/. TUBE allows to calculate the ionization source density and leakage currents in a cylindrical grid in dependence on the neutral gas influx as well as on plasma parameters. The wall geometry may be composed as a sequence of cones and cylinders. Up to now TUBE is capable of simulating the time-independent, coupled transport of H atoms and H_2 molecules. Analogously as in the fast ion transport code the plasma is considered as independent background the density and temperature of which must be given by (r,z)-profiles. In the transport simulation this space dependence is taken into consideration by the δ-impact technique /36/. For the proposed parameters the neutral atoms interact with the plasma by two types of ionizing collisions: electron impact with free electrons and charge-exchange with plasma ions. Molecules are dissociated by electrons in various reactions.

Neglecting the short transport of the intermediate product H_2^+ they are lumped in one effective process producing hydrogen atoms and ions /37/. The calculations have shown that the transport of molecules must not be neglected.

The goal of the proposed gas injection is to feed the plasma in the central cell avoiding significant increase the neutral particle density in this region. Therefore the generated ion current in the corresponding direction should be maximized whereas the gas puffing rate minimized. In the calculations the device was modelled as an open metallic tube of a certain length and diameter enclosing the target plasma and located between the mirror coil and the turning points of the fast ions (see Fig.1.) The hydrogen gas is injected through a ring-shaped gap in the mid-plane of the tube wall. Fig.23 shows results of calculations for several aperture angles of the tube. They all apply to the same energy spectrum of the hydrogen gas influx and to the same plasma parameters. For the evaluation of the results one additional fact is of importance. The density peak of the fast ions in the region of their turning points generates a peak of the electrostatic ambipolar potential in the central cell. For the standard regime of the prototype the height of this potential is expected to amount to about 1.5 times the plasma temperature T_0. Therefore, the central cell will be fed only by those ions having a kinetic energy of their motion along the z-direction greater than this value. The analysis of all numerical results allows to conclude that in case of the Hydrogen Prototype the proposed gas injection technique enables a sufficient plasma feeding in a certain range of plasma parameters and that there is an optimal aperture angle but only with a slight gain in efficiency.

The next step of the code development will be directed to the solution of neutral gas problems at the GDT facility. At the same time it makes possible to validate the physical models by comparing with these experimental results. For that purpose the time dependence of the neutral gas transport simulation and of the plasma description has to be incorporated.

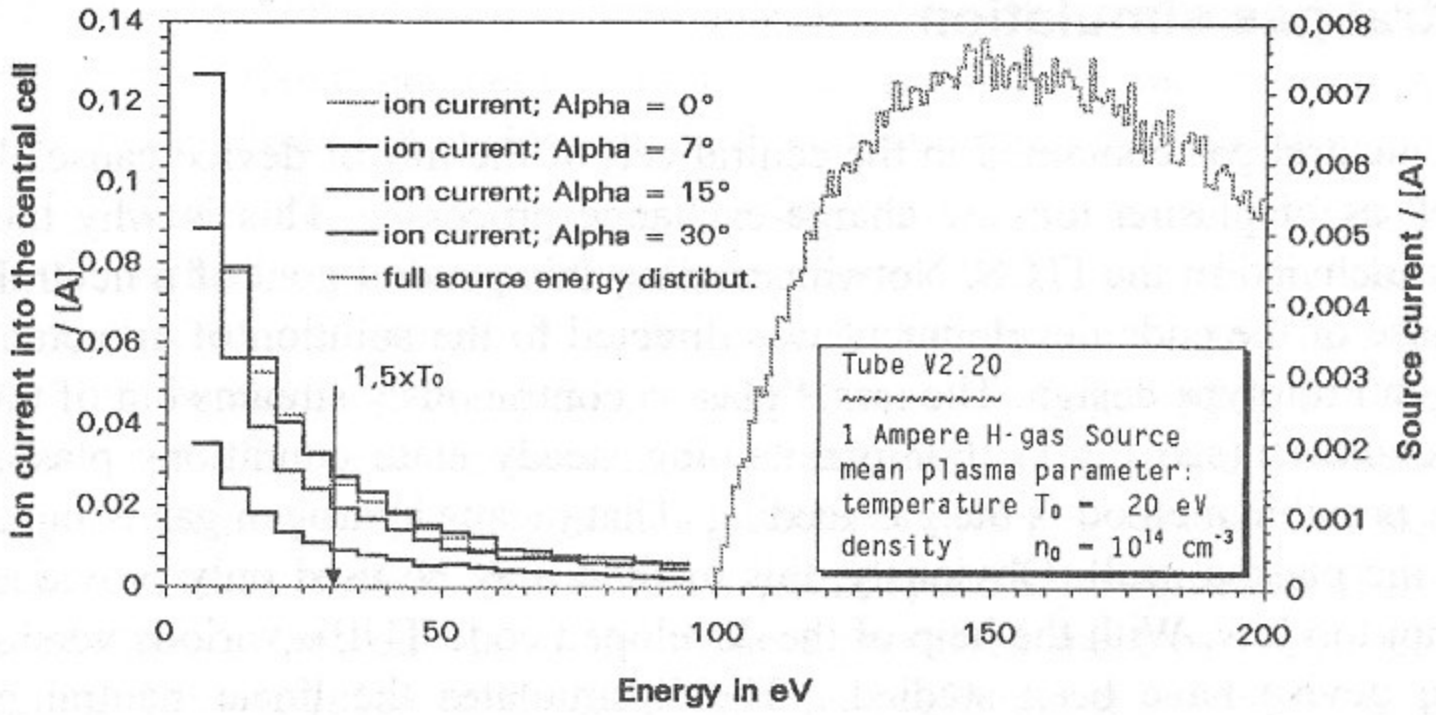

Fig.23 Ion current into the central cell in dependence on the kinetic energy of their motion along the z-direction

The code TUBE is written in FORTRAN 77 and does not require any special soft - or hardware. For this end, the codes have to be modified to meet the GDT conditions. Furthermore, the experience in the code application has shown the need to develop more efficient algorithms without essential loss in accuracy.

5.2 Simulation of non-adiabasity effects

To get a high efficiency of the neutron generator the losses of fast ions must be minimized. In this respect the question of the adiabaticity of their motion plays a decisive role. The magnetic moment of a gyrating ion is only an adiabatic invariant of its motion, i. e. does not remain exactly constant but varies to a certain degree. This effect means physically that the pitch angle (the angle between the ion flight direction and the axis of the system) changes in course of their motion between the mirrors. In magnetic fields with stronger gradients the deflection of the flight direction vector from its initial value may accumulate even up to the point when the direction vector reaches the loss cone. Then the ion flies through the mirror throat out of the system. This effect was numerically studied for the Hydrogen Prototype with the magnetic field according to the present design given in Fig. 3. Fig.24 represents the results. The magnetic field components B_z and B_r/r are the on axis values. The fluctuating curves show the variations $\delta\mu/\mu_0$ for different ions that have been started with the same initial values in the midplane. For the proton and deuteron the variations are enclosed by a well defined envelope whereas the triton does not exhibit this acceptable behaviour but indicates the approach to instability. Detailed investigations have shown that this effect is caused by relatively high values of the second spatial derivatives in the magnetic field. Furthermore, it has been demonstrated that by an appropriate rearranging of the field coils this undesired effect can be suppressed. The results of this study suggest an inspection of the adiabaticity problem in the neutron generator pre-design with the help of the same numerical method.

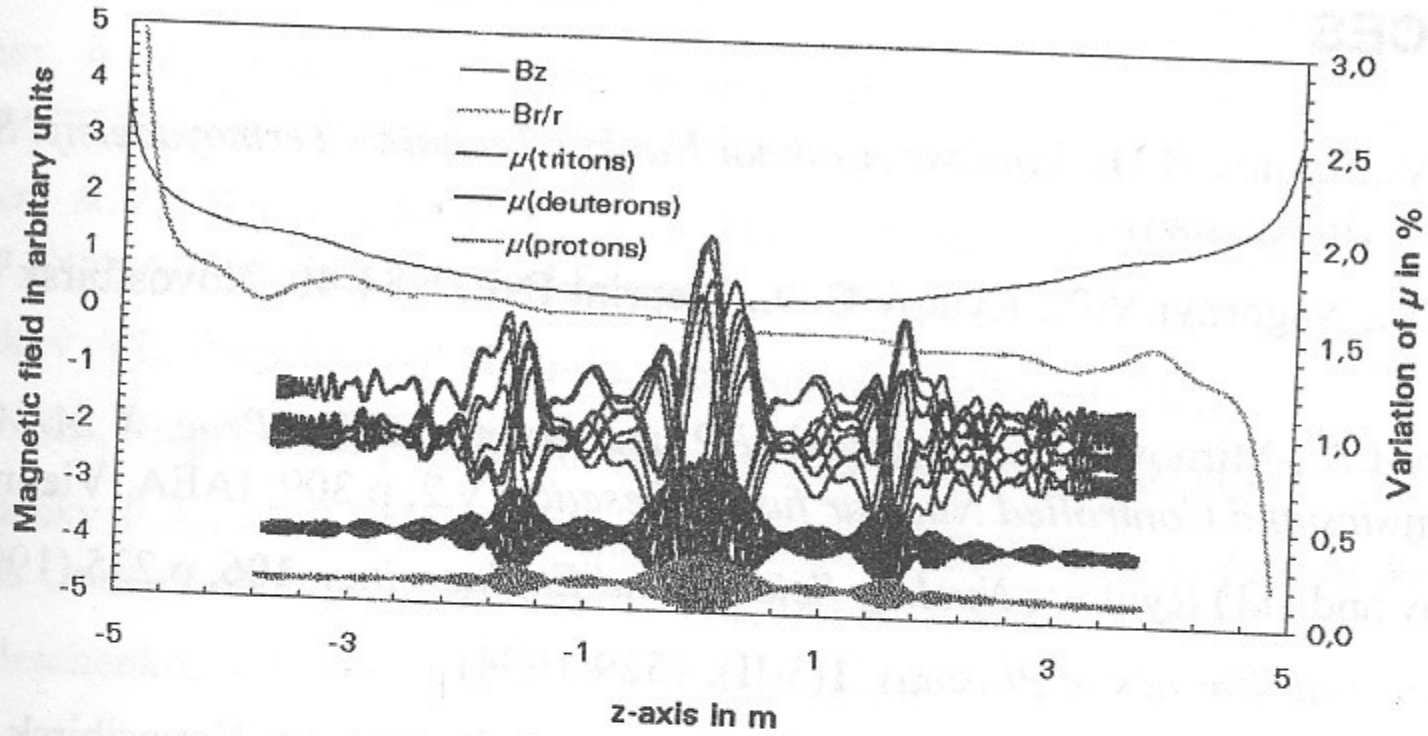

Fig.24 Variation of the magnetic moment in the Hydrogen Prototype.

Acknolegments

This work has been supported in part by INTAS through a reseach grant #93-0613, and also by the Federal Ministry of Science and Technology of the Federal Republic of Germany through a research contract code FZR 199333 mediated by FZ Rossendorf. The authors would like to express their appreciation to Prof.Collatz for his calculations of non-adiabatical effects in ion motion in the HPNS.

REFERENCES

1. Mirnov V.V., Ryutov D.D., *Voprosy Atomnoi Nauki i Techniki- Termoyadernyi Sintez*, 1-5 (1980), p.57. (in Russian)
2. Mirnov V.V., Nagornyj V.P., Ryutov D.D., Preprint INP, N84-40, Novosibirsk (1984).(in Russian)
3. Kotel'nikov I.A., Mirnov V.V., Nagornyj V.P. and Ryutov D.D., *Proc. X IAEA Conf. on Plasma Physics and Controlled Nuclear fusion Reseach.* v.2, p.309, IAEA, Vienna (1985)
4. A.A.Ivanov and D.D.Ryutov , *Nuclear Science and Engineering,* **106**, p.235 (1990)
5. A.A.Ivanov *et al, Physics of Plasmas,* **1**(5-II), 1529(1994)
6. Mirnov V.V., Nagornyj V.P., Ryutov D.D., Preprint INP, N84-40, Novosibirsk (1984) (in Russian)
7. Correll D.L., Clauser J.F., Coensgen F.H. *et al, Nuclear Fusion*, v.20, 655 (1980)
8. F.H.Coensgen, T.A.Casper, *et al*., UCRL 97280, Rev.1, LLNL (1987)
9. F.H.Coensgen, J.F.Clauser, *et al*., *Proc. 6th. IAEA Conf. on Plasma Phys. and Controlled Nucl. Fusion Res.,* Vol.3, p.135(1977)
10. T.C.Simonen (ed.) *Summary of Results from Tandem Mirror Experiment (TMX),* UCRL 53120, Livermore (1981)
11. H.L.Berk, D.D.Ryutov, *Comments Plasma Phys. Controlled Fusion* **13**, 173 (1990)
12. A.M.Lansky and D.D.Ryutov, *Proc. of Int. Conference on Open Systems for Magnetic Fusion*, p.115 Novosibirsk, World Scientific (1993)
13. Kotelnikov I.A., Ryutov D.D., Tsidulko Yu.A., Kat'ishev V.V., Komin A.V., Krivosheev V.M., Preprint INP, N90-105, Novosibirsk (1990). (in Russian)
14. Rosenbluth M.N., Longmire C.L. 1957 *Ann. Phys*. **1** 20
15. Abdrashitov G.F., Volosov V.V., Schreiner K.K., *Voprosy Atomnoi Nauki i Techniki - Termoyadernyi Sintez*, 4-1 (1981) p.19. (in Russian)
16. Davydenko V.I., Ivanov A.A., *et al*.,Preprint INP, N86-104, Novosibirsk(1986) (in Russian)
17. Persov M.V., Livshitz, Schreiner K.K., Khrestolyubov V.S., Kuznetsov G.F., *IEEE Trans. on Magnetics*, 28, 1(1992)p.255.
18. Voropaev S.G., Gorbovsky, Knyazev B.A., Lebedev S.V., Nikolaev V.S., Sheglov M.A., Preprint INP, N85-107, Novosibirsk(1985). (in Russian)
19. Ryutov D.D., Stupakov G.V. 1978 *Doklady Acad. Nauk USSR* vol 240, p 1086 (in Russian)
20. Kotelnikov I.A., Preprint INP N 83-36, Novosibirsk (1983) (in Russian)
21. Kotelnikov I.A. Preprint INP N 88-74, Novosibirsk (1988) (in Russian)
22. Rosenbluth M.N., Krall N.A., Rostoker N. 1962 *Nucl. Fusion*: supplement Part 1, p 143
23. Ryutov D.D. 1992 (unpublished)

24.Nagornyj V.P., Ryutov D.D., Stupakov G.V., *Nuclear Fusion*, 4, 24, 11(1984) p.1421.

25.Anikeev A V, *et al., Proc. International Conference on Open Plasma Confinement Systems for Fusion* (Novosibirsk 1993) World Scientific, p 303.

26.Anikeev A.V., Bagryansky P.A., *et al.,Proc. of Int. Conf. on Open Systems for Mag. Fusion* (Novosibirsk 1993) World Scientific, p.283.

27.Shetnikov A.I., Preprint INP N 86-46, Novosibirsk (1986) (in Russian)..

28.Dimov G.I., Preprint INP, N87-150, Novosibirsk(1987) (in Russian).

29.Bagryansky P.A., *et al, Plasma Physics and Controlled Nuclear Fusion Research* (Proc. 13th Int. Conf.-Washington, DC 1990), v. 2, IAEA, Vienna, (1991) p. 456.

30.Yu.I. Belchenko, V.I. Davidenko, G.E. Derevyankin, *et al., Rev. Sci. Instr.*, **61**(1) (1990) p.378.

31.N.Semashko *et al*, *Proc. of 8th Symp. on Eng. Prob. of Fusion Research*, (San. Francisco), (1979) p.221.

32.V.Bocharov, S.Konstantinov, S.Kravchenko, A.Kudryavtsev, O.Myskin, V.Panasyuk, *Proc. of Int. Conf. on Open Systems for Mag. Fusion* (Novosibirsk,1993), World Scientific, p.359.

33.R. W. Hockney and J. W. Eastwood, *"Computer Simulation using Particles"*, Adam Hilger, Bristol and New York, (1988).

34.C.K. Birdsall and A. B. Langdon, *"Plasma Physics via Computer Simulation"*, Adam Hilger, Bristol and New York, (1991).

35.D. Reiter, *"Randschicht-Konfiguration von Tokamaks: Entwicklung und Anwendung stochastischer Modelle zur Beschreibung des Neutralgastransports"*, Report Jül-1947, Juelich, (1984).

36.I. Lux, L. Koblinger, *"Monte Carlo Particle Transport Methods: Neutron and Photon Calculations"*, Boca Raton, Ann Abor and Boston, (1991).

37.R. K. Janev, W. D. Langer, K. Evans and D. E. Post, *"Elementary Processes in Hydrogen-Helium Plasmas", Springer Series on Atoms an Plasmas*, v.4, Springer-Verlag, Berlin and Heidelberg, (1987).

A.I.Gorbovsky, V.V.Mishagin, V.H.Lev, V.Y.Kremyansky, A.V.Sitnikov, K.K.Schreiner, M.V.Tauber, G.F.Abdrashitov, A.V.Anikeev, E.D.Bender, P.A.Bagryansky, A.A.Ivanov, A.N.Karpushov, A.M.Kudryavtsev, I.A.Kotel'nikov, E.P.Kruglyakov, I.M.Lansky, A.A.Pod'minogin, V.M.Panasyuk, S.D.Kravchenko, V.N.Bocharov, S.G.Konstantinov, O.K.Myskin, A.I.Rogozin, D.D.Ryutov, Yu.S.Popov, V.I.Volosov, Yu.N.Yudin, and Yu.A.Tsidulko, H.Kumpf, K.Noack, G.Otto, St.Krahl, V.Robouch

Hydrogen prototype of a plasma neutron source

А.И. Горбовский, В.В. Мишанин, В.Х. Лев, В.Ю. Кремянский и др.

Водородный прототип плазменного нейтронного источника

Budker INP 95-90

Ответственный за выпуск С.Г. Попов
Работа поступила 2.11 1995 г.

Сдано в набор 8.11. 1995 г.
Подписано в печать 8.11 1995 г.
Формат бумаги 60×90 1/16 Объем 2,6 печ.л., 2,1 уч.-изд.л.
Тираж 200 экз. Бесплатно. Заказ N 90

Обработано на IBM PC и отпечатано на
ротапринте ГНЦ РФ "ИЯФ им. Г.И. Будкера СО РАН",
Новосибирск, 630090, пр. академика Лаврентьева, 11.